DEFECT CORRECTION METHODS FOR COMPUTATIONAL AEROACOUSTICS

LIANG SIMON LAI

A thesis submitted in partial fulfilment of the
requirements of the University of Greenwich
for the Degree of Doctor of Philosophy

April 2013

DECLARATION

I certify that this work has not been accepted in substance for any degree, and is not concurrently being submitted for any degree other than that of Doctor of Philosophy being studied at the University of Greenwich. I also declare that this work is the result of my own investigations except where otherwise identified by references and that I have not plagiarised the work of others.

Student:

Liang Simon Lai

Supervisor:

Professor Choi-Hong Lai

Second Supervisors:

Dr. Georgi Djambazov

Professor Koulis Pericleous

ACKNOWLEDGEMENTS

The author wishes to express his gratitude to the University of Greenwich for the sponsorship of this research.

I would like to thank my supervisors Professor Choi-Hong Lai, Dr. Georgi Djambazov and Professor Koulis Pericleous for their concern and guidance during the various stages of the research process.

I would like to thank Professor Frédéric Magoulès, Ecole Centrale Paris, France, for allowing me to use his Helmholtz code in one of the numerical experiments.

I am also grateful to CHAM Ltd for allowing the use of their code PHOENICS in this research.

Last but not least, I would like to thank my wife Annie for her understanding, patience and care, and my family for their full support. To them all, I dedicate this thesis.

Liang Simon Lai

London, UK

2013

ABSTRACT

The idea of Defect Correction Method (DCM) has been around for a long time. It can be used in a number of different ways and can be applied to solve various linear and non-linear problems. Most defect correction related methods were used in conjunction with discretisation methods and two-level multigrid methods. This thesis examines how various iterative methods, both for linear and nonlinear problems, may be built into a unified framework through the use of defect correction. The framework is extended to the area of Computational Aeroacoustics (CAA) where sound waves generated by the pressure fluctuations are typically several orders of magnitude smaller than the pressure variations in the main flow field that accounts for flow acceleration. A decomposition of variables is used to break down the components of a typical flow variable into (1) the mean flow, (2) flow perturbations or aerodynamic sources of sound, and (3) the acoustic perturbation. The framework as discussed in this thesis would incorporate such variable decomposition. The basic principle of DCM can be applied to recover the propagating acoustic perturbation through a coupling technique. This provides an excellent concept in the re-use of existing commercial CFD software based on the framework and in the retrieval of acoustic pressure. Numerical examples demonstrating the defect correction framework for a typical car sun-roof problem was examined with promising numerical results. To this end the complete process of coupling Reynolds average Navier-Stokes and the Helmholtz equation is also presented using the DCM framework.

The DCM framework is also extended to handle higher order numerical methods for the numerical solutions of partial differential equations leading to an easy re-use of existing software approximating derivatives with a lower order discretisation. Numerical experiments were performed to demonstrate the capability of the DCM framework. It is also used to a simplified 2-D problems aiming at the understanding of Large Eddy Simulation (LES) and filtering techniques. To this end the framework of DCM leads to an efficient and robust software implementation for many CFD and aeroacoustic computation in a simple nutshell.

CONTENTS

FIGURES

TABLES

ACRONYM

APE	Acoustic Perturbation Equations
BEM	Boundary Element Method
BGK	Bhatnagar-Gross-Krook
CAA	Computational Aeroacoustics
CFD	Computational Fluid Dynamics
CFL	Courant–Friedrichs–Lewy
CPU	Central Processing Unit
DCM	Defect Correction Method
DNS	Direct Numerical Simulation
FFT	Fast Fourier Transform
FVM	Finite Volume Method
FW-H	Ffowcs Williams-Hawkings
IDeC	Iterative Defect Correction
ILES	Implicit Large Eddy Simulation
LBM	Lattice Boltzmann Method
LEE	Linearized Euler Equations
LES	Large Eddy Simulation
ODEs	Ordinary Differential Equations
PDEs	Partial Differential Equations
RANS	Reynolds-Averaged-Navier-Stokes Equations
RNG	Re-Normalisation Group
SGS	Sub-Grid cale

SPL	Sound Pressure Level

Chapter 1 INTRODUCION

Given a mathematical problem with an approximate solution, the residue or defect may be defined as a quantity that may be used to measure how well the problem has been solved. Such information may then be used in a simplified version of the original mathematical problem to provide an appropriate correction quantity. The correction can then be applied to correct the approximate solution in order to obtain a better approximate solution to the original mathematical problem. Such idea has been around for a long time and in fact has been used in a number of different ways.

This chapter gives a brief introduction to the concept of DCM and how it can be applied to solve various linear and non-linear problems. The objectives and an outline of this thesis are presented at the end of this chapter.

1.1 The Defect Correction Concept

The term "defect correction" can be introduced to characterize a class of methods for the improvement of an approximate solution of an operator equation. This class of methods includes many well-known techniques, such as Newton's method, which may be used to improve an approximate solution of a given operator equation by an iterative scheme.

Defect correction is also a very useful method for solving differential equations. Most early papers concerning defect corrections point to the work of Fox [Fox, 1947] as the first example of using defect corrections for the solution of ODEs. The work of Fox focused mainly on the solution of boundary value ODEs and PDEs.

Defect corrections have seen far less use in methods for initial value ODEs. Zadunaisky may have been the first to use deferred corrections in this context in his work concerning the accuracy of numerical approximation of orbits [Zadunaisky, 1964, 1976]. These ideas were analysed and incorporated into numerical methods in early papers by Stetter [Stetter, 1974] and Frank and Ueberhuber [Frank, Ueberhuber, 1977]. Deferred correction method is the predecessor form of DCM with further iterative technique improvement.

The defect correction approach in its basic idea can be explained as below:

For a given mathematical problem and a given approximate solution,

- define the *defect* as a quantity which indicates how well the problem has been solved, i.e. the residual of the approximate solution when it is substituted into the mathematical problem,
- use this information in a simplified version of the problem, the defect correction equation, to obtain an appropriate *correction* quantity,
- apply this correction to the approximate solution to obtain a new (better) approximate solution.

Naturally, the procedure may be repeated until the defect, which can be used as a stopping criterion in the iterative scheme, becomes small enough to be neglected.

1.2 Some Historical Examples of the DCM

One prototype of the DCM is the classical procedure for the calculation of a zero of a nonlinear equation of a single variable. An approximation $\tilde{x}$ of the solution x of the nonlinear function

$$F(x) = 0 \tag{1.2.1}$$

is substituted into F; the value of $F(\tilde{x})$ is defined as the defect. A simplified version of (1.2.1) that yields the correction v to $\tilde{x}$ is some local linearization such as the Newton linearisation

$$F(\tilde{x}) + vF'(\tilde{x}) = 0, \tag{1.2.2}$$

where $v = x - \tilde{x}$ is known as the correction. Here (1.2.2) is the defect correction equation. The method is to repeat the above steps in order to obtain a better refined approximate solution where $F'(\tilde{x})$ is updated at every step of the iterative process.

Another well-known prototype is the "iterative refinement method" ("Nachiteration"), which is an iterative method proposed by Wilkinson [Wilkinson, 1963] used to improve the accuracy of the numerical solution to systems of linear equations. When solving a system of linear algebraic equations

$$A\underline{x} = \underline{b}, \tag{1.2.3}$$

due to the presence of rounding errors, the computed solution, from a direct solution procedure, or an approximate solution, $\underline{\tilde{x}}$, has an unknown round-off contamination. Hence, there is the defect

$$\underline{r} := \underline{b} - A\underline{\tilde{x}} \neq 0. \tag{1.2.4}$$

Subtracting $A\underline{\tilde{x}}$ on both side of equation (1.2.3), one obtains

$$A(\underline{x} - \underline{\tilde{x}}) = \underline{b} - A\underline{\tilde{x}}, \tag{1.2.5}$$

such that

$$A\underline{v} = \underline{r} \tag{1.2.6}$$

where $\underline{v} = \underline{x} - \underline{\tilde{x}}$ is the correction. Then the previous solution process is used once more to compute $\underline{v}$ from (1.2.6) so that $\underline{\tilde{\tilde{x}}} = \underline{\tilde{x}} + \underline{v}$. The disadvantage here is that the problem (1.2.6) is as difficult as the one in (1.2.3). In other words, a simplified version of the original problem is not created in this process.

Consider a general operator equation

$$Lu = f \tag{1.2.7}$$

where L is a linear operator and f is a given function. The operator L is either a linear differential operator or its discretised representation. It is possible to split L into two parts, i.e. L_1 and L_2. The given equation can then be rewritten as

$$(L_1 + L_2)u = f, \tag{1.2.8}$$

re-arranging to give

$$L_1 u = f - L_2 u. \tag{1.2.9}$$

Using certain generic notation, an iterative scheme for (1.2.7) becomes

$$L_1 u_{NEW} = f - L_2 u_{OLD}. \tag{1.2.10}$$

For linear operator, subtracting $L_1 u_{OLD}$ on both side of (1.2.10) leads to

$$L_1(u_{NEW} - u_{OLD}) = f - L_2 u_{OLD} - L_1 u_{OLD}, \tag{1.2.11}$$

i.e.

$$L_1 v = f - (L_1 + L_2) u_{OLD}, \tag{1.2.12}$$

hence the defect correction equation

$$v = {L_1}^{-1} r \tag{1.2.13}$$

where

$$r = f - L u_{OLD}. \tag{1.2.14}$$

Unlike the linear algebraic system in the previous example where there is no other choice of a simpler problem, the inverse of L_1 is usually chosen to be easier to compute. After finding v from the simpler problem (1.2.13), the new iterative approximation is obtained by calculating $u_{NEW} = u_{OLD} + v$. This process can be done iteratively until v or r satisfies certain stopping criterion.

1.3 Further Applications in Different Context

1.3.1 Jacobi and Gauss-Seidel Methods

In numerical linear algebra, the Jacobi method is an iterative algorithm for determining the solutions of a system of linear equations for diagonal dominant matrices. Each equation is re-arranged so that the diagonal dominant term is made the subject. Following the splitting concept as discussed in (1.2.8), two classical iterative methods, Jacobi and Gauss-Seidel methods, are presented in terms of the defect correction concept.

Given the system of n linear equations

$$Ax = b \tag{1.3.1}$$

where $A = \begin{bmatrix} a_{11} & a_{12} & \cdots & a_{1n} \\ a_{21} & a_{22} & \cdots & a_{2n} \\ \vdots & \vdots & \ddots & \vdots \\ a_{n1} & a_{n2} & \cdots & a_{nn} \end{bmatrix}$, $x = \begin{bmatrix} x_1 \\ x_2 \\ \vdots \\ x_n \end{bmatrix}$, $b = \begin{bmatrix} b_1 \\ b_2 \\ \vdots \\ b_n \end{bmatrix}$. Then A can be decomposed into a diagonal component D and an off diagonal component R:

$$A = D + R \tag{1.3.2}$$

where $D = \begin{bmatrix} a_{11} & 0 & \cdots & 0 \\ 0 & a_{22} & \cdots & 0 \\ \vdots & \vdots & \ddots & \vdots \\ 0 & 0 & \cdots & a_{nn} \end{bmatrix}$ and $R = \begin{bmatrix} 0 & a_{12} & \cdots & a_{1n} \\ a_{21} & 0 & \cdots & a_{2n} \\ \vdots & \vdots & \ddots & \vdots \\ a_{n1} & a_{n2} & \cdots & 0 \end{bmatrix}$. Hence,

$$(D + R)x = b \tag{1.3.3}$$

In an iterative scheme, where superscript k denotes the number of iterations, (1.3.3) becomes

$$Dx^{k+1} = b - Rx^k. \tag{1.3.4}$$

Subtracting Dx^k on both side

$$D(x^{k+1} - x^k) = b - Rx^k - Dx^k. \tag{1.3.5}$$

Hence, the simplified problem for Jacobi iterative method is

$$Dv = b - Ax^k, \tag{1.3.6}$$

i.e.

$$v = D^{-1}r^k, \tag{1.3.7}$$

where the residual $r^k = b - Ax^k$ and the new iterative approximation can be calculated as $x^{k+1} = x^k + v$. The element-based formula is given by

$$x_i{}^{k+1} = x_i{}^k + \frac{1}{a_{ii}}(b_i - \sum_{j=1}^{j=n} a_{ij}\, x_i{}^k) \tag{1.3.8}$$

where $i = 1,2, \ldots, n$. Note that the computation of $x_i{}^{k+1}$ requires each element in x^k except itself.

For Gauss-Seidel method, A is split differently into a lower triangular component L_*, and a strictly upper triangular component U:

$$A = L_* + U \tag{1.3.9}$$

where $L_* = \begin{bmatrix} a_{11} & 0 & \cdots & 0 \\ a_{21} & a_{22} & \cdots & 0 \\ \vdots & \vdots & \ddots & \vdots \\ a_{n1} & a_{n2} & \cdots & a_{nn} \end{bmatrix}$ and $U = \begin{bmatrix} 0 & a_{12} & \cdots & a_{1n} \\ 0 & 0 & \cdots & a_{2n} \\ \vdots & \vdots & \ddots & \vdots \\ 0 & 0 & \cdots & 0 \end{bmatrix}$, hence

$$(L_* + U)x = b \text{ or } L_*x = b - Ux. \tag{1.3.10}$$

The Gauss–Seidel method is an iterative technique that solves the left hand side of this expression for x, using previous value for x on the right hand side. This may be written as

$$(L_*)x^{k+1} = b - Ux^k. \tag{1.3.11}$$

Subtracting L_*x^k on both side

$$L_*(x^{k+1} - x^k) = b - Ux^k - L_*x^k. \tag{1.3.12}$$

Hence,

$$v = {L_*}^{-1}(b - Ax^k), \tag{1.3.13}$$

in order to obtain $x^{k+1} = x^k + v$.

When splitting A in (1.3.9), by taking advantage of the triangular form of L_*, it uses previously computed results as soon as they are available. Hence, the elements of x^{k+1} can be computed sequentially using forward substitution:

$${x_i}^{k+1} = {x_i}^k + \frac{1}{a_{ii}}(b_i - \sum_{j<i} a_{ij}\,{x_j}^{k+1} - \sum_{j>i} a_{ij}\,{x_j}^k) \tag{1.3.14}$$

where $i = 1,2,\dots,n$.

1.3.2 Newton's Method

This section examines an application of the defect correction concept to a nonlinear system of equations consisting of two equations with two unknowns.

$$f_i(x_1, x_2) = 0; \qquad i = 1,2. \tag{1.3.15}$$

Let $\underline{x} = [x_1 \;\; x_2]^T$. The above equation may be written as

$$f_i(\underline{x}) = 0; \qquad i = 1,2. \tag{1.3.16}$$

As in the single variable case an initial approximation $\underline{x}^{(0)} = [x_1{}^{(0)} \quad x_2{}^{(0)}]^T$ is used in seeking an improved approximation $\underline{x}^{(1)} = \underline{x}^{(0)} + \Delta\underline{x}$, where $\underline{x}^{(1)} = [x_1^{(1)} \quad x_2^{(1)}]^T$, $\Delta\underline{x} = [\Delta x_1 \quad \Delta x_2 \quad]^T$ and $x_i{}^{(1)} = x_i{}^{(0)} + \Delta x_i$.

Apply the concept of the Taylor series expansion – see the derivation below using functions of two variables as an example. If the truncation of the series takes place immediately after the first derivative terms of the series, one obtains

$$f_i(\underline{x}_0 + \Delta\underline{x}) \equiv 0 \approx f_i(\underline{x}) + \sum_{j=1}^{j=2} \Delta x_j \frac{\partial f_i(\underline{x}_0)}{\partial x_j} + \frac{1}{2!}\sum_{j=1}^{j=2}\left(\Delta x_j \frac{\partial}{\partial x_j}\right)^2 f_i(\underline{x}_0) + \cdots +$$

$$\frac{1}{m!}\sum_{j=1}^{j=2}\left(\Delta x_j \frac{\partial}{\partial x_j}\right)^m f_i(\underline{x}_0); \tag{1.3.17}$$

where $i = 1{,}2$. Hence,

$$\sum_{j=1}^{j=2} \Delta x_j \frac{\partial f_i(\underline{x}_0)}{\partial x_j} \approx -f_i(\underline{x}); \qquad i = 1{,}2. \tag{1.3.18}$$

In matrix form equation (1.3.18) can be written as a simpler form of the original nonlinear system, i.e.

$$J\Delta\underline{x} = -\underline{f} \tag{1.3.19}$$

where $\underline{f} = \begin{pmatrix} f_1(\underline{x}) \\ f_2(\underline{x}) \end{pmatrix}$ and J is known as the Jacobian. Therefore, the correction $\Delta\underline{x}$ can be calculated as

$$\Delta\underline{x} = -J^{-1}\underline{f}, \tag{1.3.20}$$

and the new iterative approximation is calculated as $x_i^{(1)} = x_i^{(0)} + \Delta x_i$. Equation (1.3.20) also applies to the case of n equations.

1.3.3 Solving Nonlinear Differential Equations

This section considers a defect correction approach for the solutions of nonlinear differential equations.

Consider a given functional equation $F(u, u', u'') = 0$ which describes a nonlinear second order differential equation. Let $s = (u \quad u' \quad u'')^t$ be the exact solution, $\tilde{s} = (\tilde{u} \quad \tilde{u}' \quad \tilde{u}'')^t$ be an approximate solution, and $V = (v \quad v' \quad v'')^t = s - \tilde{s}$ be the

correction. Note that $F(\tilde{u}, \tilde{u}', \tilde{u}'') \neq 0$. Expand $F(\tilde{u} + v, \tilde{u}' + v', \tilde{u}'' + v'')$ up to the first order term leads to

$$F(\tilde{u} + v, \tilde{u}' + v', \tilde{u}'' + v'') = F(\tilde{u}, \tilde{u}', \tilde{u}'') + \left(\frac{\partial F}{\partial \tilde{u}} v + \frac{\partial F}{\partial \tilde{u}'} v' + \frac{\partial F}{\partial \tilde{u}''} v''\right) \equiv 0, \quad (1.3.21)$$

where high order terms are ignored. The above equation is rearranged to a linearised equation given by

$$\frac{\partial F}{\partial \tilde{u}} v + \frac{\partial F}{\partial \tilde{u}'} v' + \frac{\partial F}{\partial \tilde{u}''} v'' = -F(\tilde{u}, \tilde{u}', \tilde{u}''). \quad (1.3.22)$$

Equation (1.3.22) is a linear differential equation involving the correction term v. Analytical or numerical solution may be obtained by solving the defect correction equation (1.3.22). An improved approximation can be obtained by $\tilde{\tilde{s}} = \tilde{s} + v$, or $\tilde{\tilde{u}} = \tilde{u} + v$, $\tilde{\tilde{u}}' = \tilde{u}' + v'$, $\tilde{\tilde{u}}'' = \tilde{u}'' + v''$.

Using a generic notation for iteration, the example below is used to illustrate the above method.

$$F(u, u', u'') = u'' - f(u, u', u'')u' = 0, \quad (1.3.23)$$

where $u = u(x)$ .Let $v = u^{k+1} - u^k$; $v' = u'^{k+1} - u'^k$; $v'' = u''^{k+1} - u''^k$. Equation (1.3.22) is rewritten in the simplified form as

$$F^k + \frac{\partial F^k}{\partial u^k} v + \frac{\partial F^k}{\partial u'^k} v' + \frac{\partial F^k}{\partial u''^k} v'' = 0, \quad (1.3.24)$$

where $F^k = F(u^k, u'^k, u''^k)$ and u^k is the k th iterative approximation of u. The derivative terms for the example in equation (1.3.23) are given as below:

$$\frac{\partial F^k}{\partial u^k} = -\frac{\partial f^k}{\partial u^k} u'^k;$$

$$\frac{\partial F^k}{\partial u'^k} = -\frac{\partial f^k}{\partial u'^k} u'^k - f^k;$$

$$\frac{\partial F^k}{\partial u''^k} = 1.$$

Hence (1.3.24) becomes

$$F^k + \left(-\frac{\partial f^k}{\partial u^k} u'^k\right) v + \left(-\frac{\partial f^k}{\partial u'^k} u'^k - f^k\right) v' + v'' = 0. \quad (1.3.25)$$

Then calculate v such that

$$v'' + \left(-\frac{\partial f^k}{\partial u'^k} u'^k - f^k\right) v' + \left(-\frac{\partial f^k}{\partial u^k} u'^k\right) v = -F^k, \quad (1.3.26)$$

subject to homogeneous boundary conditions. Finally the iterative approximations can be obtained as

$$u^{k+1} = u^k + v$$

$$u'^{k+1} = u'^k + v'$$

$$u''^{k+1} = u''^k + v''.$$

1.3.4 Ordinary Differential Equations

The defect correction concept has an equivalent form known as the deferred correction can be applied to first order ordinary differential equations. It takes a low order scheme in obtaining an approximate solution and projects it to a high order scheme by calculating the residual and solving for the correction.

The classical defect correction procedure was developed by Pereyra [Pereyra, 1966, 1969]. The deferred correction procedure was developed in Dutt, Greengard & Rokhlin [Dutt et al, 2000]. The latter procedure is discussed here.

Consider the initial value problem

$$y'(t) = f(t, y(t)) \tag{1.3.27}$$

with initial value $y(0) = y_0$ is used here to demonstrate the concept.

Let $y(t)$ denote the exact solution to (1.3.27). A time integration numerical method with step length Δt yields u_j, an approximate solution to $y((j-1)\Delta t)$, with $u_0 = y_0$. A continuous interpolate $u(t)$ from the discrete values u_j can be built. Define the residual/defect

$$r(t) = f\big(t, u(t)\big) - u'(t), \tag{1.3.28}$$

which is used to measure how well $u(t)$ satisfies (1.3.27).

The correction $v(t) = y(t) - u(t)$ also satisfies an initial value problem, given by

$$\begin{aligned} v'(t) &= y'(t) - u'(t) \\ &= f\big(t, y(t)\big) - f\big(t, u(t)\big) + r(t) \\ &= f(t, u(t) + v(t)) - f\big(t, u(t)\big) + r(t) \\ &= F(t, u(t), v(t)) + r(t) \end{aligned} \tag{1.3.29}$$

with initial value $v(0) = 0$, where $F(t,u,v) = f(t,u+v) - f(t,u)$. The defect correction problem given in (1.3.29) is of the same form as (1.3.27) and it can be solved using the same numerical method, to obtain an approximation $\tilde{v}$ to v. The solution update is thus $u_{NEW} = u(t) + \tilde{v}(t)$. The method depends on the choice of F and its approximation $u(t)$.

1.3.5 Multi-Scale Problems

Many problems of fundamental and practical importance are of multi-scale nature. As a typical example, the velocity field in turbulent transport problems fluctuates randomly and contains many scales depending on the Reynolds number of the flow. Another example of multi-scale problems can refer to a system that consist of a large-scale/main stream and a small-scale/noise component, where the small-scale component is much smaller than the large-scale component by magnitude. The system as a whole can be difficult to solve. One technique is to separate the two components and obtain an approximate solution assuming the small-scale component is negligible, then apply DCM in order to use the same or simplified solver to solve the correction term using the small-scale component.

Consider the linear system in (1.3.1) with the r.h.s. being perturbed with the noise $\epsilon b'$, i.e.

$$Ax = b + \epsilon b', \tag{1.3.30}$$

where ϵ is a small parameter. Suppose the unperturbed system

$$A\tilde{x} = b, \tag{1.3.31}$$

is solved leading to the solution $\tilde{x} = A^{-1}b$. $\tilde{x}$ is obviously very close to the solution of (1.3.30). Computing the defect

$$r = b + \epsilon b' - A\tilde{x}, \tag{1.3.32}$$

leads to

$$r = \epsilon b'. \tag{1.3.33}$$

Comparing the two solutions $\tilde{x}$and x by subtracting Equation (1.3.31) from (1.3.30), i.e.

$$A(x - \tilde{x}) = \epsilon b'. \tag{1.3.34}$$

Putting $v = x - \tilde{x}$ leads to $A(v) = \epsilon b'$ where the solution is

$$v = \epsilon A^{-1} b'. \tag{1.3.35}$$

The true solution of the perturbed linear system in (1.3.30) can be retrieved as $x = \tilde{x} + v$.

The above concept can easily be demonstrated by using a linear system of equations given here:

$$\begin{pmatrix} 2 & 3 & 1 \\ 5 & 6 & 4 \\ 3 & 2 & 0.2 \end{pmatrix} \begin{pmatrix} x \\ y \\ z \end{pmatrix} = \begin{pmatrix} 4.001 \\ 6.001 \\ 2.001 \end{pmatrix}, \tag{1.3.36}$$

which can be rewritten in the form of Equation (1.3.30)

$$\begin{pmatrix} 2 & 3 & 1 \\ 5 & 6 & 4 \\ 3 & 2 & 0.2 \end{pmatrix} \begin{pmatrix} x \\ y \\ z \end{pmatrix} = \begin{pmatrix} 4 \\ 6 \\ 2 \end{pmatrix} + 0.001 \begin{pmatrix} 1 \\ 1 \\ 1 \end{pmatrix}. \tag{1.3.37}$$

In many applications there are problems where the matrix elements may be contaminated with noise such as $\epsilon A'$. Equation (1.3.1) can be rewritten as

$$(A + \epsilon A')x = b, \tag{1.3.38}$$

where $\epsilon A'$ is known as the noise. Again, the unperturbed system

$$A\tilde{x} = b, \tag{1.3.39}$$

has solution $\tilde{x} = A^{-1} b$ which is close to the exact solution of (1.3.38). The defect can be calculated as

$$r = b - (A + \epsilon A')\tilde{x}, \tag{1.3.40}$$

hence

$$r = -\epsilon A' \tilde{x}. \tag{1.3.41}$$

Subtracting Equation (1.3.39) from (1.3.38) leads to the defect correction equation:

$$Av = r, \tag{1.3.42}$$

where $v = x - \tilde{x}$. The above problem can be solved in an iterative manner, until r is small enough to be neglected. Note that the defect correction equation $Av = r$ is no more simpler in terms of the solution process compare to the original unperturbed problem.

The above concept can be demonstrated with the example below.

$$\begin{pmatrix} 2.003 & 3.001 & 1.001 \\ 5 & 6.002 & 4 \\ 3.003 & 2 & 0.205 \end{pmatrix}\begin{pmatrix} x \\ y \\ z \end{pmatrix} = \begin{pmatrix} 1 \\ 1 \\ 1 \end{pmatrix} \tag{1.3.43}$$

which is rewritten in the form of Equation (1.3.38)

$$\begin{pmatrix} 2 & 3 & 1 \\ 5 & 6 & 4 \\ 3 & 2 & 0.2 \end{pmatrix}\begin{pmatrix} x \\ y \\ z \end{pmatrix} + 0.001\begin{pmatrix} 3 & 1 & 1 \\ 0 & 2 & 0 \\ 3 & 0 & 5 \end{pmatrix}\begin{pmatrix} x \\ y \\ z \end{pmatrix} = \begin{pmatrix} 1 \\ 1 \\ 1 \end{pmatrix}. \tag{1.3.44}$$

The DCM can be easily adapted to problems which exhibit multiple scale solutions. Here is a perturbed first order differential equation

$$\frac{du}{dt} = -1 - \epsilon u, \tag{1.3.45}$$

subject to the initial condition $u(0) = 1$ that is used to illustrate the idea. The solution of (1.3.35) exhibits multi-scale behaviour. A series solution such as $u = \sum_{i=0}^{i=\infty} u_i$ is usually used to represent such solution. Here the DCM is demonstrated using a finite series such as

$$u = u_0 + u_1 + u_2 + u_3, \tag{1.3.47}$$

where $u_0 \gg u_1 \gg u_2 \gg u_3$. Assuming it is possible to solve

$$\frac{du}{dt} = f(t), \tag{1.3.46}$$

subject to suitable initial condition, and $f(t)$ is a function of t only.

Step 1: Obtain the solution of the unperturbed problem,

$$\frac{du_0}{dt} = -1, \tag{1.3.48}$$

with initial value $u_0(0) = 1$. Integrating (1.3.48) with respect to t leads to

$$u_0(t) = 1 - t. \tag{1.3.49}$$

The defect/residual of the solution u_0 can be calculated as

$$\begin{aligned} r &= -1 - \epsilon u_0 - \frac{\mathrm{d}u_0}{\mathrm{dt}} \\ &= -1 - \epsilon(1 - t) - (-1) \\ &= \epsilon(t - 1). \end{aligned} \tag{1.3.50}$$

Step 2: Solve the defect correction problem

$$\frac{du_1}{dt} = r = \epsilon(t - 1), \tag{1.3.51}$$

with initial value $u_1(0) = 0$. Integrating (1.3.51) with respect to t leads to

$$u_1(t) = \epsilon(\frac{t^2}{2} - t). \tag{1.3.52}$$

$u_1(t)$ is considered as the correction to u_0, hence the new approximation solution u becomes

$$u^{NEW} = u_0 + u_1 = 1 - t + \epsilon\left(\frac{t^2}{2} - t\right), \tag{1.3.53}$$

and

$$\frac{du^{NEW}}{dt} = -1 + \epsilon(t - 1). \tag{1.3.54}$$

Hence the defect due to u^{NEW} is

$$\begin{aligned} r &= -1 - \epsilon u^{NEW} - \frac{\mathrm{du}^{NEW}}{\mathrm{dt}} \\ &= -1 - \epsilon\left[1 - t - \epsilon\left(\frac{t^2}{2} - t\right)\right] - [-1 + \epsilon(t - 1)] \\ &= \epsilon^2(t - \frac{t^2}{2}). \end{aligned} \tag{1.3.55}$$

Step 3: Solve yet another defect correction problem

$$\frac{du_2}{dt} = r = \epsilon^2(t - \frac{t^2}{2}), \tag{1.3.56}$$

with initial value $u_2(0) = 0$. Integrating (1.3.56) with respect to t leads to

$$u_2(t) = \epsilon^2(\frac{t^2}{2} - \frac{t^3}{6}). \tag{1.3.57}$$

Hence the new approximate is

$$u^{NEW} = u_0 + u_1 + u_2 = 1 - t + \epsilon\left(\frac{t^2}{2} - t\right) + \epsilon^2(\frac{t^2}{2} - \frac{t^3}{6}), \tag{1.3.58}$$

and that

$$\frac{du^{NEW}}{dt} = -1 + \epsilon(t - 1) + \epsilon^2(t - \frac{t^2}{2}). \tag{1.3.59}$$

Hence the defect is

$$\begin{aligned} r &= -1 - \epsilon u^{NEW} - \frac{du^{NEW}}{dt} \\ &= \epsilon^3(\frac{t^3}{6} - \frac{t^2}{2}). \end{aligned} \tag{1.3.60}$$

Step 4: solve

$$\frac{du_3}{dt} = r = \epsilon^3(\frac{t^3}{6} - \frac{t^2}{2}), \tag{1.3.61}$$

with initial value $u_3(0) = 0$. Integrating (1.3.61) with respect to t leads to

$$u_3(t) = \epsilon^3(\frac{t^4}{24} - \frac{t^3}{6}). \tag{1.3.62}$$

Finally the latest updated solution becomes

$$\begin{aligned} u^{NEW} &= u_0 + u_1 + u_2 + u_3 \\ &= 1 - t + \epsilon\left(\frac{t^2}{2} - t\right) + \epsilon^2\left(\frac{t^2}{2} - \frac{t^3}{6}\right) + \epsilon^3(\frac{t^4}{24} - \frac{t^3}{6}). \end{aligned} \tag{1.3.63}$$

The process may be carried on until terms of high order ϵ are very small. Note that (1.3.63) provides an understanding of the properties of the solution in terms on ϵ and the dependence of t in terms of ϵ.

1.4 General Defect Correction Principle

Several important applications of the defect correction concept are discussed in the previous section. It can be seem that the steps involved in the DCM may be easily automated in a computational environment. In this section an attempt is made to present a general framework such that various applications discussed so far may be studied under the framework. It is hoped that this framework may also be used with suitable modification for aeroacoustics and some related fluid dynamics and numerical algorithms.

Consider the general problem

$$Lu = f, \tag{1.4.1}$$

where L is an operator, linear or non-linear, u is a function defined over certain domain Ω and f is defined on Ω. For example L could be a linear or non-linear differential operator, or some finite difference replacement of a differential operator. Let u^* be the solution of the problem in (1.4.1).

Assuming that (1.4.1) cannot be solved directly but an approximate solution $\tilde{u} \in \Omega$ may be evaluated. The defect can then be calculated as

$$r(\tilde{u}) := f - L\tilde{u}. \tag{1.4.2}$$

Furthermore, as described by Bohmer and Stetter [Böhmer, Stetter, 1984], assuming that the approximate problem

$$\tilde{L}u = \tilde{f} \tag{1.4.3}$$

can be solved for $\tilde{f}$, i.e. that the solution operator $\tilde{G}$ of (1.4.3) exists and is an approximate inverse of L such that

$$\tilde{G}(L\tilde{u}) \approx \tilde{u} \tag{1.4.4}$$

and

$$L(\tilde{G}(\tilde{u})) \approx \tilde{u}. \tag{1.4.5}$$

Now assuming some approximation $\tilde{u}$ for u^* is given and that its defect (1.4.2) has been computed. In the general nonlinear case, there are two ways to use this information for the computation of an improved approximation $\tilde{\tilde{u}}$ by means of solving an approximate problem defined in (1.4.3).

(A) Compute the change v in the solution of (1.4.3) when the right hand side f is changed by $r(\tilde{u})$. Then use v as a correction to $\tilde{u}$, i.e. transfer the observed change to the target problem (1.4.1):

$$\tilde{\tilde{u}} := \tilde{u} + v = \tilde{u} + [\tilde{G}(f) - \tilde{G}\big(f - r(\tilde{u})\big)], \tag{1.4.6}$$

and using (1.4.2) to obtain

$$\tilde{\tilde{u}} = \tilde{u} + \tilde{G}(f) - \tilde{G}(L\tilde{u}). \tag{1.4.7}$$

(B) Generate an equation (1.4.3) with solution $\tilde{u}$ and change its right-hand side $\tilde{l} = \tilde{L}\tilde{u}$ by $r(\tilde{u})$. Then take the solution of this modified equation as $\tilde{\tilde{u}}$, i.e. again transfer the effect observed for (1.4.3) to the target problem (1.4.1):

$$\tilde{\tilde{l}} := \tilde{l} + r(\tilde{u}) = \tilde{l} + f - L\left(\tilde{G}\big(\tilde{l}\big)\right),$$

$$\tilde{\tilde{u}} := \tilde{G}\left(\tilde{\tilde{l}}\right) = \tilde{G}\big[\big(\tilde{L} - L\big)\tilde{u} + f\big]. \tag{1.4.8}$$

Note that it is the existence of $\tilde{G}$ and not of $\tilde{L} = \tilde{G}^{-1}$ which is essential, as is immediately clear from (1.4.7) and (1.4.8). In some respect, versions (A) and (B) appear dual to each other.

In both approaches, the arising problems with modified right-hand sides are often called neighbouring problems [Auzinger et al, 2002]. In the context of this thesis it is

also known as the defect correction equation/problem or the simplified problem. In some applications, the operator $\tilde{L} - L$ in (1.4.8) is much simpler than either $\tilde{L}$ or L so that there is an advantage in using approach (B).

The success of the basic defect correction steps (1.4.7) or (1.4.8) depends on the contractivity of the operations $\left(I - \tilde{G}(L)\right)$ or $\left(I - L\left(\tilde{G}\right)\right)$ respectively, since (1.4.7) implies

$$\tilde{\tilde{u}} - u^* = \left(I - \tilde{G}(L)\right)\tilde{u} - (I - \tilde{G}(L))u^* \tag{1.4.9}$$

while (1.4.8) implies, with $\tilde{G}(l^*) = u^*$,

$$\tilde{\tilde{l}} - l^* = \left(I - L\left(\tilde{G}\right)\right)\tilde{l} - (I - L\left(\tilde{G}\right))l^*. \tag{1.4.10}$$

The contractivity is, of course, closely related to the approximate inverse property of $\tilde{G}$, cf. (1.4.4) and (1.4.5) respectively.

The element $\tilde{\tilde{u}}$ which is gained through defect correction may be used in two ways:

- interpret $\tilde{u} - \tilde{\tilde{u}}$ as an estimate of the error $\tilde{u} - u^*$ of the original approximation $\tilde{u}$
- subject $\tilde{\tilde{u}}$ as the new approximation to another defect correction step.

The iterative use of the basic defect correction procedures (1.4.7) or (1.4.8) leads to the Iterative Defect Correction (IDeC) algorithms of Stetter [Stetter, 1974]:

(A) $$u^{(k+1)} := u^{(k)} + \tilde{G}(f) - \tilde{G}\left(Lu^{(k)}\right), \tag{1.4.11}$$

(B) $$l^{(k+1)} := l^{(k)} + f - L\left(\tilde{G}\left(l^{(k)}\right)\right), \text{ with } u^{(k)} = \tilde{G}\left(l^{(k)}\right); \tag{1.4.12}$$

for injective $\tilde{G}$, (1.4.12) turns into

$$u^{(k+1)} := \tilde{G}[\left(\tilde{L} - L\right)u^{(k)} + f]. \tag{1.4.13}$$

Usual starting values for these iterations are $u^{(0)} = \tilde{G}(f)$ and $l^{(0)}$ =f.

1.5 Objectives

The main objectives of this thesis are as follows:

1) Develop a general framework of the DCM for nonlinear problems.
2) Examine an application of the general framework for aeroacoustic problems.
3) Build a suitable and efficient coupling procedure, in order to incorporate the source-extraction formulation, between a finite-volume based CFD solver and the Helmholtz equation solver.
4) Examine the use of the general framework for high order schemes and its filtering effect in large eddy simulation.
5) Highlight the possibility of using the defect correction concept in the development of new high order schemes and their robust implementation within an existing CFD environment.

1.6 Outline of the Thesis

The remaining part of the thesis is organized as follows. In Chapter 2, a brief overview is given of computational aeroacoustics. This includes several existing techniques that are currently being practiced in the aeroacoustic industry. In Chapter 3, a general framework based on the defect correction concept is developed for continuous problems with aeroacoustic applications in mind. Chapter 4 examines an application of the DCM to aeroacoustics noise analysis. The analysis concerns a sunroof buffeting problem and its related software coupling involved in the acoustic study. In Chapter 5, the defect correction framework is applied to high order schemes with the emphases on robust software development. The framework is also extended to handle turbulence through filtering analysis. A summary and some suggestions of future work of this research are made in Chapter 6.

Chapter 2 SOME ASPECTS OF COMPUTATIONAL AEROACOUSTICS

This chapter gives a brief overview of aeroacoustic and solution strategies of computational aeroacoustics. Shortcomings of the current techniques that are normally used by researchers in Computational Aeroacoustics are discussed. A brief comparison between Computational Aeroacoustics and conventional Computational Fluid Dynamics is made. Some difficulties and challenges faced in the development of Computational Aeroacoustics are pointed out. Current computational strategies used in Computational Aeroacoustics are discussed. The importance of adopting coupling methods for practical aeroacoustic prediction is particularly emphasized through the analysis of the characteristics in both the unsteady flow field and the acoustic field.

2.1 Acoustics and Aeroacoustics

Hearing is one of the most crucial means of survival in the animal world, and speech is one of the most distinctive characteristics of human development and culture. So it is no surprise that the science of acoustics spreads across so many facets of our society – music, medicine, architecture, industrial production, warfare and more. Art, craft, science and technology have provoked one another to advance the whole, as in many other fields of knowledge.

The word "acoustic" is derived from the Greek word ἀκουστικός (akoustikos), meaning "of or for hearing, ready to hear". Acoustics is originally the study of small pressure waves in a medium that can be detected by the human ear, which is also referring to, *sound*.

The sensation of sound is produced primarily by variations in air pressure that are detected by the mechanical effect on the tympana (ear drums) of human auditory system. Motion of each tympanum relates to the physiology and psychophysics of the hearing process, e.g. Stevens and Davis [Stevens, Davis, 1983] and Gulick [Gulick, 1971], is not related to this thesis. The important point is the generation of air pressure variation due to fluid flows.

In general, there are two types of sound can be distinguished: pleasant ones and disturbing ones. The former can be referred to as harmonic and melodious music, while roaring from engines could refer to the later, or the so-called *noise*. One kind of sound measurement is frequency with the unit Hz which is pronounced as "Hertz". Frequency measures cycles of something happening, i.e. frequency of the same thing occurring. A wheel goes around one time in one second is known as an Hz. If a sound wave goes up and down, that is one Hz. Directly translated into sound, an Hz is one vibration. Sound waves are mechanical waves that can cause the sensation of hearing. In fluids such as air and water, sound waves propagate as disturbances in the ambient pressure level. While this disturbance is usually small, it is still noticeable to the human ear. The smallest sound that a person can hear is nine orders of magnitude smaller than the ambient pressure. The loudness of these disturbances is called the sound pressure level, and is measured on a logarithmic scale in decibels (dB). These waves are produced by bodies vibrating at frequencies lying between the range of 12Hz and 20,000Hz, perceived by the human ear. This is known as the audible range of frequency. In terms of wavelength, this range extends from about 17m to 1.7cm. Mechanical waves of frequency lesser than 12Hz or greater than 20,000Hz are inaudible and are called infrasonic and ultrasonic, respectively. The seismic waves are infrasonic waves. Bats, dolphins and submarines make use of ultrasonic to find their way in the dark. The word acoustic refers to both the audible range and infrasonic/ultrasonic, i.e. the entire frequency range without limit. In addition to frequency, the study of sound is conventionally divided, according to the propagation medium, into aeroacoustics, solid acoustics and underwater acoustics. In this thesis, the formation and the propagation of sound in fluids, particularly in the air, are considered.

Aeroacoustics, also referred as the science of aerodynamic sound, deals with the type of sound generated by oscillating vortex structures or pressure fluctuations in the airflow, as well as with the propagation of the resulting acoustic waves through non-uniformly

moving medium. In other words, aeroacoustics is the scientific study of sound generation created directly by the turbulent fluid motion or by aerodynamic forces interacting with surfaces. A practical aeroacoustic analysis relies upon the so-called Acoustic Analogy, where the governing equitation of motion of the fluid are coerced into a form reminiscent of the wave equation of "classical" (i.e. linear) acoustics. The objectives of aeroacoustics are to understand the physics of aerodynamic sound generation, to develop effective and accurate prediction and analysis method, and ultimately, to reduce the noise level which emitted from jet engine or by any other unit with high-unsteady flow.

Aeroacoustics had long been a part of aerodynamics and had not become an independent field of research until the early fifties of the twentieth century this scientific discipline was initiated by Lighthill [Lighthill, 1952]. He was stimulated by anticipating large-scale commercial jet air travel to formulate his successful theory of jet noise which has stood the tests of time and of far-reaching extension. Flow noise has subsequently become a matter of serious military concern in the operation and detection of ships and submarines, and the aeronautical and naval applications of flow-noise theory between them cover a wide range of interesting phenomena. With proper manipulation of the Euler equations, he derived a wave equation based on pressure as the fluctuating variable, and the flow variables contributing to the source of fluctuation. The resulting wave equation can then be integrated with the help of Green's Function [Green, 1828], or can be integrated numerically. Thus, this equation can represent the sound propagation from a source in an ambient condition. The important work of Lighthill is now widely considered as the birth of aeroacoustics as an independent field of research. With the success of the acoustic analogy, many improvements were made on the derivation of the wave equation. From 1950s to mid- 1980s, most works are based on a very small number of well-known theoretical approaches, which are modified, simplified, and adapted to the particular flow conditions (some of the most popular versions of Lighthill's acoustic analogy include the Ffowcs-Williams and Hawkings equation [Ffowcs–William, Hawkings, 1969], Lilley's equations [Lilley, 1974], as well as diverse forms of Kirchhoff's theorem , e.g., Pilon and Lirintzis, [Pilon, Lirintzis, 1998]).

It is well-known to all that the reduction of the aerodynamic noise is very important for civil aeroplanes. The flow-induced noise is also one of the principal concerns for military aircrafts. For high-speed fighter aircrafts, the vibration of structural loads, which partly results from the flow-induced aeroacoustic environment, on the vehicle and on

weapons that may be in the vicinity of the aircraft, should be taken into account. The several dB reduction of sound pressure level could gain an obvious increase of the fatigue life of a particular vehicle.

In order to be able to compete with air traffic on short distance, high speed trains have to become faster, and the need to reduce the aerodynamic noise is true for future high speed trains. With the era of widespread supersonic flight and the proliferation of general aviation aircraft on future horizons, the noise generated by aircraft is of great concern for communities near airports, for passengers in the aircraft's cabin, and for the structural integrity of the airframe. In addition, there are a number of situations that desire lower noise including underwater vehicles, wind turbines, and helicopter rotors.

2.2 Computational Aeroacoustics

There are three distinct streams in the study of aeroacoustics: analytical methods, experimental methods and numerical methods.

Before the development of large memory and high-speed computers, the study of aeroacoustic problems was mainly based on the first two methods mentioned above, or empirical approaches combined with both theoretical methods and experimental methods. With rapid advancement in computational power and significant strides in numerical algorithm development, many problems in scientific and engineering fields have been studied using the computer as a tool. Consequently, many new branches of research have been generated, such as, computational mathematics, computational physics, computational chemistry, and so on. Similarly, the dramatically increasing in numerical investigations for aeroacoustic problems led to a research field, Computational Aeroacoustics (CAA), which deals with the direct calculation of acoustic field generated by flow and of the interaction with flow. Probably the term *Computational Aeroacoustics* entered the field with a publication of Hardin and Lamkin [Hardin, Lamkin, 1984], who claimed, that *"… the field of computational fluid mechanics has been advancing rapidly in the past few years and now offers the hope that "computational aeroacoustics," where noise is computed directly from a first principles determination of continuous velocity and vorticity fields, might be possible, …"*

There are many challenges for CAA due to the fact that the physics behind the unsteadiness that generates aerodynamic sound is very complicated. For instance, energy that is radiated as noise is typically only a small fraction of the total energy near the acoustic source. This is part of the scale disparity between acoustic and hydrodynamic fluctuations. Because there is a factor of about 10^6 between the acoustic pressure at the threshold of audibility and the limit of intolerable overload for the human ear, and because within that range subjective response is more logarithmic than linear, and some research indicate that it is even more complicated, e.g., Gulick [Gulick, 1971] and Rossing [Rossing, 1982]. Therefore, it is convenient to do something similar for acoustic pressures. Therefore the sound pressure level (SPL or L_p) for an acoustic pressure p can be defined as $L_p = 20\log_{10}\left(p'_{rms}/p_{ref}\right)$ with units of decibels (dB). The reference pressure $p_{ref} = 20\times10^{-6}$ Pa, ($20\,\mu$Pa), is approximately the threshold of human hearing in its most sensitive range from 1 to 3 kHz, and p'_{rms} is the root mean square of the acoustic pressure perturbations. The ratio of pressure amplitudes between a quiet conversation, 60dB, and a rock 'n' roll concert, 120dB, is 1000 [$60 = 20 * \log_{10}\left(p_{conversation}/p_{ref}\right)$ and $120 = 20 * \log_{10}\left(p_{concert}/p_{ref}\right)$, therefore $p_{concert} = 10\text{^}3 * p_{conversation}$]. In addition, atmospheric pressure is 3500 times greater than the pressure amplitude of a 120dB signal. At 120dB, one starts feeling discomfort and experiences a ringing in the ears. Although this level is very loud to human ears, it is so small that a typical computational fluid dynamics (CFD) simulation very easily loses the sound waves among the large hydrodynamic fluctuations. Simultaneously resolving the hydrodynamic fluctuations and the wide range of acoustic signals is very difficult.

From the perspective of physics, there are two fundamental problems in CAA that can be classified. One is to model numerically acoustic sources in the unsteady flows as accurate as possible, so one can determine the acoustic signal at any point in the flow; the other is to compute accurately the propagation/radiation of the resulting acoustic waves. Although both the flow field and the accompanying acoustic field are governed by the same equations of motion of fluids --- the unsteady compressible Navier-Stokes equations, one must recognize that acoustic perturbations are several orders of magnitude smaller than the mean quantities of flow. Understanding the source of the noise itself, its manifestation in the near-field and propagation to the far-field are all critical in the development of future noise reduction technologies.

2.3 Solution strategies in CAA

Aeroacoustic problems are by nature very different from standard aerodynamics and fluid mechanics problems. These differences pose a number of major challenges to CAA. A few of the important computational challenges are listed below:

(a) Aeroacoustics problems, by definition, are time dependent, whereas aerodynamics and fluid mechanics problems may be time independent or involve only low frequency unsteadiness.

(b) Aeroacoustics problems typically involve frequency range that spreads over a wide bandwidth. Numerical resolution of the high frequency waves with extremely short wavelengths becomes a formidable obstacle to accurate numerical simulation.

(c) Acoustic waves usually have small amplitudes. They are very small compared to the mean flow. Often, the sound intensity is five to six orders smaller [Tam, 2001]. To compute sound waves accurately, a numerical scheme must have extremely low numerical noise.

(d) In most aeroacoustics problems, interest is in the sound waves radiating to the far field. This requires a solution that is uniformly valid from the source region all the way to the measurement point at many acoustic wavelengths away. Because of the long propagation distance, CAA schemes must have minimal numerical dispersion and dissipation. Also, it should propagate the waves at the correct wave speeds and is isotropic irrespective of the orientation of the computation mesh.

(e) In general, flow disturbances in aerodynamics or fluid mechanics problems tend to decay very fast away from a body or their source of generation. Acoustic waves, on the other hand, decay very slowly and actually reach the boundaries of a finite computation domain. To avoid the reflection of outgoing sound waves back into the computation domain, and thus contaminates the numerical solution, radiation boundary conditions must be imposed at the artificial exterior boundaries to assist the waves to exit

smoothly. For standard CFD problems, such boundary conditions are usually not required.

(f) Aeroacoustics problems are archetypical examples of multiple-scales problems. The length scale of the acoustic source is usually very different from the acoustic wavelength. CAA methods must be able to deal with problems with greatly different length scales in different parts of the computational domain.

It must be acknowledged that CFD has been very successful in solving fluid and aerodynamics problems. CFD methods are generally designed for low frequency of unsteadiness or steady state problems. Because of the tremendous success of CFD, it is tempting to use these methods to solve aeroacoustics problems as well. In the past, there have been a number of attempts to do just that. However, the results have proven to be quite discouraging. For example, Hsi and Perie [Hsi, Perie, 1977] tried to use a commercial CFD code RADIOSS to solve the sound scattering problems of the Second CAA Workshop on Benchmark Problems. The results were disastrous. The computed results were highly dispersive and differed significantly from the exact solutions.

As discussed above, it is clear that the nature of aeroacoustics problems is substantially different from those of traditional fluid dynamics and aerodynamics problems. To be able to compute or simulate aeroacoustics problems accurately and efficiently, standard CFD schemes, designed for applications to fluid problems, are generally not adequate. For this reason there has been an independent development of CAA and various computational methods have been developed.

From a computational viewpoint, the current research community and industry practice have two solution strategies, i.e. the direct sound computation and coupling computation of sound.

2.3.1 Direct Sound Computation

One of the prediction strategies in CAA is direct computation of sound. The unsteady flow of an aerodynamic problem and the sound generated by such unsteadiness can be computed together using the unsteady compressible Navier-Stokes equation, i.e. the unsteady flow and its sound are regarded as correlated parts of the same flow field. Such

direct computations of aerodynamic sound generation allow a detailed understanding of practically any flow quantity of interest. Modelling the mechanism of sound generation can be explored at a fundamental level. There are mainly three different approaches which are normally used by researchers in CAA. By placing them in the decreasing order in terms of accuracy as well as computational costs, they are direct numerical simulation (DNS), Large Eddy Simulation (LES) and Reynolds-averaged-Navier-Stokes equations (RANS).

(A) Direct Numerical Simulation

There are two principal ways of obtaining theoretical results regarding turbulence, namely turbulence theory and solution of the Navier-Stokes Equations. In 1972, Orszag and Patterson were the first to introduce the name of Direct Numerical Simulation (DNS) [Orszag, Patterson, 1972]. DNS is to solve the primitive variable of the Navier-Stokes Equations numerically without using any turbulence model. This means that the whole range of spatial and temporal scales of the turbulence must be resolved. All the spatial scales of the turbulence must be resolved in the computational mesh, from the smallest dissipative scales, η (Kolmogorov microscales), up to the integral scale, L, with the motions containing most of the kinetic energy. The Kolmogorov scale, η, at which viscosity dominates and the turbulent kinetic energy is dissipated into heat, is given by $\eta = \left(\nu^3 / \varepsilon\right)^{1/4}$, where ν is the kinematic viscosity and ε is the rate of kinetic energy dissipation. On the other hand, the integral scale depends usually on the spatial scale of the boundary conditions. To satisfy these resolution requirements, the number of points N along a given mesh direction with mesh size h, must be $Nh > L$, so that the integral scale is contained within the computational domain, and also $h \le \eta$, so that the Kolmogorov scale can be resolved. Since $\varepsilon \approx u'^3 / L$, where u' is the root mean square of the velocity, the previous relations imply that a three-dimensional DNS requires a number of mesh points N^3 satisfying $N^3 \ge Re^{9/4} = Re^{2.25}$, where Re is the turbulent Reynolds number: $Re = \frac{u'L}{\nu}$. Therefore the memory storage requirement in a DNS grows very fast with the Reynolds number. In addition, given the very large memory requirement, the integration of the solution along temporal axis must be done by an explicit method. This means that in order to be accurate, the integration must be done

with a time step, Δt, small enough such that a fluid particle moves only a fraction of the mesh spacing h in each step. Typically the condition $C = \frac{u'\Delta t}{h} < 1$, where C is the Courant number, must be satisfied. The total time interval simulated is generally proportional to the turbulence time scale τ given by $\tau = \frac{L}{u'}$. Combining these relations, and the fact that h must be of the order of η, the number of time-integration steps must be proportional to $L/(C\eta)$. On the other hand, from the definitions for Re, η and L as previously stated, it follows that $\frac{L}{\eta} \approx Re^{3/4}$, and consequently, the number of time steps grows also as a power law of the Reynolds number. As the number of floating-point operations required to complete the simulation is proportional to the number of mesh points and the number of time steps, therefore the number of operations grows with Re.

Although DNS is famously known as the most accurate and also the most straightforward numerical method in direct sound computation, the computational cost of DNS is very high, even at low Reynolds numbers. Due to the use of highly accurate, high-order schemes to limit dispersion and dissipation errors, these schemes tend to have little flexibility in handling complex geometries and general boundary conditions. In addition, the calculation has to discretize the equations on extremely fine grids in order to properly resolve all scales of an unsteady flow. Furthermore, the size of the smallest scales decreases will cause the increase in Reynolds number. It can be easily shown that it will be impossible to apply DNS for practical flow and aeroacoustic problems (high Reynolds number) in the foreseeable future [Launder et al, 1975].

(B) Large Eddy Simulation

Large Eddy Simulation is a numerical technique used to solve the partial differential equations governing turbulent fluid flow. It was formulated in the late 1960s and became popular in later years. It was first used by Joseph Smagorinsky to simulate atmospheric air currents, and its primary use at that time was for meteorological calculations and predictions. During the 1980s and 1990s LES became widely used in the field of engineering. LES requires less computational effort than DNS and yet it is able to deliver

a high level of detail. LES can predict instantaneous flow characteristics and resolve some larger turbulent flow structures by solving the turbulence model.

The direct numerical solution of the Navier-Stokes equations is usually intractable in turbulent flow, due to the large range of scales of motion. To reduce this range, the Navier-Stokes equations are filtered leading to the LES equations. The solution to the LES equations is now defined in a filtered velocity field, with the smaller scales of motion being filtered out of the original direct solution field. With the smaller scales eliminated from direct solution, a wider grid spacing may be used, thus lowering the computational costs. However, the effect of the smaller scales on the large scales has been ignored using this approach. Large eddies of the flow are dependent on the flow geometry, while smaller eddies are self-similar and have a universal character. For this reason, the effect of the smaller and more universal eddies on the larger ones may be modelled. Thus, in LES the large scale motions of the flow are calculated, while the effect of the smaller universal scales (the sub-grid scales) are modelled using a sub-grid scale (SGS) model. In practical implementations, one is required to solve the filtered Navier-Stokes equations with an additional sub-grid scale stress term [Nieuwstadt et al, 1993].

Consider the Navier-Stokes equations for an incompressible fluid, i.e.

$$\frac{\partial u_i}{\partial x_i} = 0 \tag{2.1}$$

$$\frac{\partial u_i}{\partial t} + \frac{\partial u_i u_j}{\partial x_j} = -\frac{1}{\rho}\frac{\partial p}{\partial x_i} + \nu \frac{\partial^2 u_i}{\partial x_i \partial x_j} \tag{2.2}$$

Let an over bar denotes filtering. The momentum equation in (2.2) after filtering becomes

$$\overline{\frac{\partial u_i}{\partial t}} + \overline{\frac{\partial u_i u_j}{\partial x_j}} = -\overline{\frac{1}{\rho}\frac{\partial p}{\partial x_i}} + \nu \overline{\frac{\partial^2 u_i}{\partial x_i \partial x_j}} \tag{2.3}$$

Assuming that filtering and differentiation commute [Vasilyev et al, 1998], the above equation becomes

$$\frac{\partial \overline{u}_i}{\partial t} + \overline{\frac{\partial u_i u_j}{\partial x_j}} = -\frac{1}{\rho}\frac{\partial \overline{p}}{\partial x_i} + \nu \frac{\partial^2 \overline{u}_i}{\partial x_i \partial x_j} \tag{2.4}$$

Let $\tau_{ij} = \overline{u_i u_j} - \bar{u}_i \bar{u}_j$ and $\frac{\partial \tau_{ij}}{\partial x_j} = \frac{\partial \overline{u_i u_j}}{\partial x_j} - \frac{\partial \bar{u}_i \bar{u}_j}{\partial x_j}$. Subtract $\frac{\partial \tau_{ij}}{\partial x_j}$ on both sides of Equation (2.4). Hence the resulting set of equations is the LES equations

$$\frac{\partial \bar{u}_i}{\partial t} + \frac{\partial \bar{u}_i \bar{u}_j}{\partial x_j} = -\frac{1}{\rho}\frac{\partial \bar{p}}{\partial x_i} + \nu \frac{\partial^2 \bar{u}_i}{\partial x_i \partial x_j} - \frac{\partial \tau_{ij}}{\partial x_j} \tag{2.5}$$

where u_i is the velocity field, p is the pressure, ρ is the density, and ν is the viscosity. The τ_{ij} term represents the SGS stress that must be modelled.

Modelling the SGS stress term τ_{ij} is one of the central problems in LES. The most commonly used SGS models are the Smagorinsky model and its variants. They compensate for the unresolved turbulent scales through the addition of an eddy viscosity into the governing equations. The basic formulation of the Smagorinsky model is

$$\tau_{ij} = -2\nu_T \bar{S}_{ij} \tag{2.6}$$

where

$$\bar{S}_{ij} = \frac{1}{2}\left(\frac{\partial \bar{u}_i}{\partial x_j} + \frac{\partial \bar{u}_j}{\partial x_i}\right) \tag{2.7}$$

is an entry of the strain rate tensor and the eddy viscosity ν_T is calculated as

$$\nu_T = (C_s \Delta_g)^2 \sqrt{2\bar{S}_{ij}\bar{S}_{ij}} \tag{2.8}$$

where Δ_g is the grid size and C_s is a constant. Many techniques have been developed to calculate C_s. Some models use a static value for C_s, often calculated from empirical experiments of similar flows to those being modelled. Other models dynamically calculate C_s as a function of space and time [Moeng, Sullivan, 2002].

Although the LES results in the literature are encouraging and show the potential promise of LES application to aeroacoustic prediction, the method has its own weaknesses. One of the weaknesses, which might affect the application of LES to sound computations, is the effect of the small scales on the acoustic sources. For example, none of the LES studies on jet noise done so far has predicted the high-frequency noise associated with the unresolved scales. The problem of evaluating the sound generation of

the unresolved, subgrid-scale motions could be alleviated or overcome by developing new subgrid-scale models.

It has also been noted that the highest Reynolds number achieved in the LES simulations, which is much higher than that attained by current DNS calculations, so far is still below those practical Reynolds number of interest ($\mathrm{Re} = O(10^6)$ to $O(10^9)$) [Breuer, 2000]. Simulations of aeroacoustic problems at higher Reynolds number (for example, jet noise) would be very useful in analysing the broadband noise spectrum at such high Reynolds numbers.

Overall, LES requires less computational effort than DNS. Although in LES the effect of small (subgrid) scale eddies on the large (resolved) scale motion is modelled, which drastically reduces the computational cost compared with DNS, the acoustic power may have been underestimated if the contribution of these unresolved (small) scales is simply neglected. While the contribution of the small scales to the momentum transport may be usually small, their contribution to the sound generation may be significant. In addition, accurate computation in time and space, fine mesh (or high-order schemes) and small time-steps are required in calculating the motion of the large scales. Since the turbulent motions are intrinsically three-dimensional, even flows that are two-dimensional or one-dimensional in the mean flow must be computed using a three-dimensional approach. Direct sound computation based on LES for application to engineering flows still remains expensive.

(C) Reynolds–Averaged Navier–Stokes Equations

Apart from the direct computation of aerodynamic sound based on DNS and LES, several direct computations of sound from the unsteady solution of Reynolds-averaged-Navier-Stokes equations (RANS) were presented by some researchers (see e.g., [Launder, Spalding, 1972] and [Launder et al, 1975]). RANS equations are time-averaged equations of motion for fluid flow. They are primarily used while dealing with turbulent flows. These equations can be used with approximations based on knowledge of the properties of flow turbulence to give approximate averaged solutions to the Navier-Stokes equations.

The basic tool required for the derivation of the RANS equations from the instantaneous Navier–Stokes equations is the Reynolds decomposition. Reynolds

decomposition is a mathematical technique to separate the average and fluctuating parts of a quantity, such as a flow variable (e.g. velocity u) into the mean (time-average) component ($\overline{u}$) and the fluctuating component ($\tilde{u}$). Previous work by Djambazov [Djambazov et al, 1998] and Wang [Wang et al, 2004] also employed such decomposition technique. In perturbation theory the similar decomposition is also employed. The defect correction framework described in Chapter 3 also rely on such decomposition. Specifically the variable u is decomposed as

$$u(X,t) = \overline{u}(X) + \tilde{u}(X,t) \tag{2.9}$$

where $X = (x, y, z)$ is the position vector.

For the current study there are three velocity components and the pressure variable, i.e. $u_i = \overline{u_i} + \tilde{u}_i$, with $i = 1,2,3$, and $p = \overline{p} + \tilde{p}$. Substituting them into the time averaged version of Equations (2.1) and (2.2) and taking into account of external and internal viscous friction/forces in the mean flow and the perturbations f leads to

$$\frac{\partial \overline{u}_i}{\partial x_i} = 0 \tag{2.10}$$

,

$$\frac{\partial \overline{u}_i}{\partial t} + \frac{\partial \overline{u}_i \overline{u}_j}{\partial x_j} + \frac{\overline{\partial \tilde{u}_i \tilde{u}_j}}{\partial x_j} = \overline{f_i} - \frac{1}{\rho}\frac{\partial \overline{p}}{\partial x_i} + \nu \frac{\partial^2 \overline{u}_i}{\partial x_i \partial x_j} \tag{2.11}$$

.

The momentum equation can also be written as,

$$\frac{\partial \overline{u}_i}{\partial t} + \frac{\partial \overline{u}_j \overline{u}_i}{\partial x_j} = \overline{f}_i - \frac{1}{\rho}\frac{\partial \overline{p}}{\partial x_i} + \nu \frac{\partial^2 \overline{u}_i}{\partial x_i \partial x_j} - \frac{\partial \overline{\tilde{u}_i \tilde{u}_j}}{\partial x_j} \tag{2.12}$$

.

On further manipulations this yields,

$$\rho \frac{\partial \overline{u}_i}{\partial t} + \rho \frac{\partial \overline{u}_j \overline{u}_i}{\partial x_j} = \rho \overline{f}_i + \frac{\partial}{\partial x_j}\left[-\overline{p}\delta_{ij} + 2\mu \overline{S}_{ij} - \rho \overline{\tilde{u}_i \tilde{u}_j} \right] \tag{2.13}$$

where, $\overline{S}_{ij} = \frac{1}{2}\left(\frac{\partial \overline{u}_i}{\partial x_j} + \frac{\partial \overline{u}_j}{\partial x_i} \right)$ is the mean rate of strain tensor.

The time derivative, $\rho \frac{\partial \overline{u_i}}{\partial t}$, can be eliminated since $\overline{u_i}$ is a time average component, which is time independent, hence,

$$\rho \frac{\partial \overline{u}_j \overline{u}_i}{\partial x_j} = \rho \overline{f}_i + \frac{\partial}{\partial x_j}\left[-\overline{p}\delta_{ij} + 2\mu \overline{S}_{ij} - \rho \overline{\widetilde{u}_i \widetilde{u}_j} \right] \tag{2.14}$$

Reynolds-averaged-Navier-Stokes equations (RANS) were examined by some researchers in several direct computations of sound. Baysal, Yen and Fouladi [Baysal et al, 1992], Shih, Hamed and Yeuan [Shih et al, 1994] have noted that direct simulations of acoustic field based on RANS cannot usually obtain reasonable acoustic results due to their excessive turbulent dissipation. Under the circumstances, researchers in computational aeroacoustics field began to seek for more practical solution strategy for the last two decades. The development of coupling methods for aeroacoustic problems has been an active area of research in CAA for many years.

2.3.2 Coupling Techniques in the Computation of Sound

The fundamental basis for the use of coupling methods comes from the observation of characteristics of the flow field and the accompanying acoustic field. Due to the distinct characteristics (an enormous range of length scales and time scales are involved) in both the unsteady flow field and the resulting acoustic field, domain decomposition technique is generally adopted. In CAA, computational domain (domain of interest) is often divided into two parts; one is the 'near field' where main acoustic sources (sound generation) are located, where detailed flow structures can be resolved by a CFD technique (DNS, LES or RANS); the other one is the 'far field' in which concerns are the propagation/radiation of the resulting acoustic waves, which is then calculated via an acoustic analogy or by solving a set of acoustic perturbation equations. The most important advantage in such a fluid-acoustic-coupling procedure is the aerodynamic calculation and the calculation of sound propagation/radiation is separated so that the most appropriate approach may be employed at each part.

There are currently two types of coupling methods under the framework of the fluid-acoustic-coupling procedure. In the first type the first step is to solve the full unsteady incompressible or compressible flow equations for the near-field of the unsteady flow by means of LES or unsteady RANS, after computing the sources of the acoustic field an acoustic integral approach, where various versions of acoustic analogies, is applied to solve the sound propagation. These include Lighthill's wave equation [Lighthill, 1952], the Ffowcs Williams-Hawkings (FW-H) equation [Ffowcs–William, Hawkings, 1969],

and Lilley's equations [Lilley, 1974]. An acoustic analogy may be derived by re-arranging the governing equations of the fluid motion such that the left-hand side consists of a wave operator in an undisturbed medium and the right-hand side is comprised of acoustic source terms. The solution of the equation can be written as the convolution of the source terms with the Green function for the wave operator. Hence, with the strengths of the source terms obtained in the regions where they are significant, one can determine the acoustic signal at any point in the flow, including locations at long distances from the sources. The acoustic analogy is the most developed method and widely used in the aircraft industry.

Take Lighthill's acoustic analogy for example. Lighthill essentially recast the exact equations of fluid motion (Navier Stokes equations and continuity equation) in the form of an inhomogeneous wave equation suitable to be applied in the far-field, therefore making it an acoustic analogy with fluid mechanics. The governing equation for the conservative form of the continuity (Equation 2.15) and momentum equation (Equation 2.16) for a compressible fluid based on a Cartesian coordinate system, ignoring body forces, may be described as

$$\frac{\partial \rho}{\partial t} + \frac{\partial (\rho u_i)}{\partial x_i} = 0 \quad , \tag{2.15}$$

$$\frac{\partial (\rho u_i)}{\partial t} + \frac{\partial (\rho u_i u_j + p_{ij})}{\partial x_j} = 0 \quad , \tag{2.16}$$

where $p_{ij} \equiv p\delta_{ij} - \tau_{ij}$. ρ is the density of the fluid, δ_{ij} is the Kronecker delta (δ_{ij} = 1 if $i = j$ and δ_{ij} = 0 otherwise), u_i and u_j are the velocity components, p_{ij} is the stress tensor and p is the static pressure. If external sources are not considered, the famous Lighthill's wave equation can be written as

$$\frac{\partial^2 \tilde{\rho}}{\partial t^2} - c_0^2 \nabla^2 \tilde{\rho} = \frac{\partial^2 T_{ij}}{\partial x_i \partial x_j} \quad , \tag{2.17}$$

where $\tilde{\rho}$ is density perturbation (defined as the deviation from the quiescent reference density), c_0 is the speed of sound in the fluid at rest that is defined as $c_0 = \frac{\gamma p}{\rho}$, where $\gamma = 1.4$ is the ratio of specific heats in a general airflow [Wood, 1946]. The Lighthill stress tensor, T_{ij} is defined as

$$T_{ij} = \rho u_i u_j - \tau_{ij} + \left(\tilde{p} - c_0^2 \tilde{\rho}\right)\delta_{ij} \tag{2.18}$$

,

and $\tilde{p}$ is pressure perturbation, τ_{ij} is the viscous stress term. Each of these acoustic source terms may play a significant role in the generation of noise depending upon flow conditions considered. It is generally accepted however, the term τ_{ij} on noise generation is in orders of magnitude less than the other terms and can be consequently neglected in most situations.

Note that perturbations ($\tilde{\rho}, \tilde{p}$) are defined as the deviations between the total flow variables (ρ, p) and the quiescent reference state (ρ_0, p_0) during the derivation of Equation 2.17, i.e.

$$\tilde{p} = p - p_0, \tag{2.19}$$

$$\tilde{\rho} = \rho - \rho_0 . \tag{2.20}$$

Another alternative is the Kirchhoff-surface method [Kirchhoff, 1883], in which the acoustic sources are determined correspondingly from the unsteady solutions in the acoustic source field. In addition, the boundary element method (BEM) can also be utilized for the prediction of far-field sound propagation/radiation in Manoha, Elias, Troff and Sagaut [Manoha et al, 1999]. For such coupling method, the most important advantage is that the calculation of acoustic field is computationally economical since certain integral formulation is used. However, the main drawback is that the details of the acoustic field cannot be obtained.

In the second type of coupling method, which has already received much attention from CAA community in the past decade, the first step in the coupling is similar to the first step of the coupling procedure described above. CFD techniques such as DNS, LES and unsteady RANS simulations as well as other appropriate methods can be used in solving the unsteady aerodynamic near-field, which contains the sound sources. For the second part of this coupling procedure, instead of using an acoustic integral approach, it makes use of the calculated sources for the solution of the acoustic field by solving a set of acoustic perturbation equations (APE) [Ewert, Schroder, 2003] associated with source terms through certain numerical methods. A typical example of acoustic perturbation equations is the linearized Euler equations (LEE) with acoustic source terms which from

the solution of RANS in the near field to predict noise radiated from axisymmetric supersonic jets has been used by Viswanathan and Sankar [Viswanathan, Sankar, 1995]. Comparing to the first type of coupling method associated with acoustic analogies, the second type of coupling method obtains more details of the acoustic field since the acoustic wave propagation in the near field is done by means of solving the APE, the same terms of which are derived from the unsteady flow field.

A coupling method, in which the near-field of the unsteady flow may be simulated by a fine-mesh-small-timestep-LES-alike numerical method applied in two-dimension, and the acoustic propagation in a medium at rest where flow motions may be neglected, may be resolved by Helmholtz equation to predict buffeting noise inside a car compartment due to aerodynamic flow over an open sunroof is mentioned in detail in the following section.

2.4 Closure

A brief overview is given of aeroacoustic and solution strategies of computational aeroacoustics. One of the objectives of this thesis is to build an efficient coupling procedure in order to incorporate the source-extraction formulation for a general aeroacoustic problem. Some of the recent industrial practices and researches have also been reviewed in later Chapter 4 in order to provide an up to date overview on how others have been dealing with the similar problem. In the next chapter, it is intended to rewrite some of the solution strategies of computational aeroacoustic under the framework of defect correction and to discuss the advantage of doing so.

Chapter 3 THE DEFECT CORRECTION FRAMEWORK FOR PROBLEMS AT THE CONTINUUM LEVEL

This chapter examines the concept of defect correction in details. The main aim of this chapter is to build a framework of the DCM for problems that exhibit multiple scales at the continuum level. This work typically examines problems that have two different scales. However the generalisation to more scales should not be a problem. A brief discussion towards the end of this chapter is given of such generalisation.

3.1 DCM for Navier-Stokes Equations without Multi-Scales

In the numerical solution of higher Reynolds number flow problems one of the most commonly reported results is that "the method failed". Often "failure" means that the iterative method used to solve the linear and/or nonlinear system for the approximate solution at the new time level failed to converge within the time constraints of the problem or the resulting approximation had poor solution quality. The first type of failure can usually be overcome easily by using an upwind or artificial viscosity discretization at the expense of decreasing dramatically the accuracy of the method and possibly even altering the predictions of the simulation at the qualitative level, therefore increasing the likelihood of the second type of failure.

One interesting approach to attaining (by a convergent method) an approximate solution of desired accuracy is the DCM. Briefly, let a k^{th} order accurate discretization of the Navier-Stokes equation be written as

$$N_h(u_h) = f, \tag{3.1.1}$$

where h is the discretisation parameter such as the spatial grid size.

Equation (3.1.1) is solved by means of adding an artificial viscosity approximation, i.e.

$$-\alpha h \Delta_h u_h^{(1)} + N_h\left(u_h^{(1)}\right) = f_0. \tag{3.1.2}$$

Hence compute the defect leads to

$$r := f - N_h\left(u_h^{(k)}\right);\ k = 1,2,3,\ldots \tag{3.1.3}$$

Construct simplified problem/defect correction equation as below

$$-\alpha h \Delta_h u_h^{(k)} + N_h\left(u_h^{(k)}\right) = f - \alpha h \Delta_h u_h^{(k-1)},\ \ for\ k = 2,3,\ldots,L \tag{3.1.4}$$

where $u_h^{(k)}$ contains variable involved in the Navier-Stokes equations.

It was demonstrated in Layton, Lee, Peterson [Layton et al, 2002] that

$$\begin{aligned} \left\| u_N - u_h^{(k)} \right\|_E &= O\left(h^k + h\left\| u_N - u_h^{(L-1)} \right\|_E\right) \\ &= O(h^k + h^L). \end{aligned} \tag{3.1.5}$$

Hence after $L = k$ steps,

$$\left\| u_N - u_h^{(k)} \right\|_E = O(h^k). \tag{3.1.6}$$

Here u_N denotes the solution of the Navier-Stokes equations..

For problems with high Reynolds number turbulence is expected. In these cases the DCM needs to be combined with appropriate turbulence models. These models tend to introduce extra nonlinearities (due to the closure of the model). It might be possible to incorporate them into the residual on the right-hand side, as was done in the quasistatic case by Ervin, Layton, Maubach [Ervin et al, 2000].

There has been an extensive study and development of this approach for equilibrium flow problems, see e.g. Hemker [Hemker et al, 1997] , Koren [Koren, 1991], Heinrichs [Heinrichs, 1996], Layton, Lee, Peterson [Layton et al, 2002], Ervin and Lee [Ervin, Lee, 2006].

There have also been some recent studies that deals with high Reynolds number problem based on defect corrections method, see [Liu, Hou, 2010] and [Qin et al, 2011].

For many years, it has been widely believed that (3.1.4) can be directly imported into implicit time discretization of flow problems in the obvious way: discretize in time.

Unfortunately, this natural idea did not seem to be even stable (see [Labovschii, 2009]). On the other hand, there is a parallel development of DCM without any use of special stabilisation (such as $-\alpha h\Delta_h$ in (3.1.4)) for initial value problems with the aim to increase the accuracy of the time discretization. This work contains no reports of instabilities: see, e.g., Heywood, Rannacher [Heywood, Rannacher, 1990], Hemker, Shishkin, Shishkina [Hemker et al, 2002], Lallemand, Koren [Lallemand, Koren, 1993], Minion [Minion, 2004]. With this parallel development and after more than thirty years of studies of (3.1.4), there has yet to be a successful extension of (3.1.4) to time dependent flow problems.

3.2 DCM for Navier-Stokes Equation with Two Scales

Most defect corrections are used in conjunction with discretisation methods and two-level multigrid methods [Böhmer, Setter, 1984]. Recall that sound waves – manifested as pressure fluctuations – are typically several orders of magnitude smaller than the pressure variations in the flow field that account for flow acceleration. Furthermore, they propagate at the speed of sound in the medium, not as a transported fluid quantity. A decomposition of variables was first introduced by Djambazov, Lai, Pericleous [Djambazov et al, 1996] and has been further examined in [Djambazov et al, 1998] to include three types of components. These components include (1) the mean flow, (2) flow perturbations or aerodynamic sources of sound, and (3) the acoustic perturbation. The accurate computation of (1) and (2) has been demonstrated in Djambazov, Lai, Pericleous [Djambazov et al, 1998]. Mathematically, the flow variable U may be written as $\overline{U} + \widetilde{U}$ where $\overline{U}$ denotes the mean flow and part of aerodynamic sources of sound and $\widetilde{U}$ denotes the remaining part of the aerodynamic sources of sound and the acoustic perturbation.

While flow perturbation or aerodynamic sources of sound may be easier to recover, it is not true for the acoustic perturbation because of its comparatively small magnitude. In fact, the solutions of the Reynolds averaged Navier-Stokes equations reveal only a truncated part of the full physical quantities. The basic principle of the defect correction can be applied to recover the propagating acoustic perturbation. The method relies on the

use of lower order partial differential equation defined on the same computational domain where a residue exists such that the acoustic perturbation may be retrieved through a properly defined coarse mesh.

The aim here is to solve the non-linear equation

$$L(U) \equiv L\left(\overline{U} + \widetilde{U}\right) = f, \tag{3.2.1}$$

where L is a non-linear operator depending on $U \equiv \overline{U} + \widetilde{U}$. It is noted that $\widetilde{U} \ll \overline{U}$. In the case of sound generated by the motion of fluid, it is natural to imagine L as the Navier-Stokes operator. For a 2-D problem,

$$\overline{U} = \begin{bmatrix} \bar{\rho} \\ \bar{u} \\ \bar{v} \end{bmatrix} \qquad \widetilde{U} = \begin{bmatrix} \tilde{\rho} \\ \tilde{u} \\ \tilde{v} \end{bmatrix}$$

where ρ is the density of fluid and u and v are the velocity components along the two spatial axes. The 2-D Navier-Stokes problem $L(U) = f$ is written as

$$\frac{\partial \rho}{\partial t} + \frac{\partial \rho u}{\partial x} + \frac{\partial \rho v}{\partial y} = 0 \tag{3.2.2}$$

and

$$\begin{cases} \frac{\partial u}{\partial t} + u\frac{\partial u}{\partial x} + v\frac{\partial u}{\partial y} + \frac{1}{\rho}\frac{\partial P}{\partial x} - \frac{f_1}{\rho} = 0 \\ \frac{\partial v}{\partial t} + u\frac{\partial v}{\partial x} + v\frac{\partial v}{\partial y} + \frac{1}{\rho}\frac{\partial P}{\partial y} - \frac{f_2}{\rho} = 0 \end{cases}, \tag{3.2.3}$$

where P is the pressure and f_i is the external and internal viscous friction in the mean flow and the perturbations along i-th axis.

Suppose (3.2.1) may be split and re-written as

$$L\left(\overline{U} + \widetilde{U}\right) \equiv L(\overline{U}) + E\{\bar{u}\}\tilde{u} + K[\bar{u}, \tilde{u}] \tag{3.2.4}$$

where $E\{\bar{u}\}$ is an operator depending on the knowledge of $\bar{u}$ and $K[\bar{u}, \tilde{u}]$ is a functional depending on the knowledge of both $\bar{u}$ and $\tilde{u}$. Following the concept of defect correction, $\bar{u}$ may be considered as an approximate solution to (3.2.1). Hence one can evaluate the residue of (3.2.1) as

$$R \equiv f - L(\overline{U}), \tag{3.2.5}$$

which may then be substituted into (3.2.4) to give

$$E\{\bar{u}\}\tilde{u} + K[\bar{u}, \tilde{u}] = R. \tag{3.2.6}$$

In many cases, $K[\bar{u},\tilde{u}]$ is small and can then be neglected. In those cases, the problem in (3.2.6) is a linear problem and may be solved more easily to obtain the acoustics fluctuation $\tilde{u}$. A non-linear iterative solver is required in order to obtain u for cases when $K[\bar{u},\tilde{u}]$ is not negligible. Finally, to obtain the approximate solution $\bar{u}$, one only needs to solve $L(\bar{U}) = f$.

Expanding $L(\bar{U} + \tilde{U}) = f$ for L being the Navier-Stokes operator and re-arranging one obtain

$$\begin{cases} \frac{\partial\tilde{\rho}}{\partial t} + \bar{u}\frac{\partial\tilde{\rho}}{\partial x} + \bar{\rho}\frac{\partial\tilde{u}}{\partial x} + \left[\tilde{u}\frac{\partial(\bar{\rho}+\tilde{\rho})}{\partial x} + \tilde{\rho}\frac{\partial(\bar{u}+\tilde{u})}{\partial x}\right] = -[\frac{\partial\bar{\rho}}{\partial t} + \bar{u}\frac{\partial\bar{\rho}}{\partial x} + \bar{\rho}\frac{\partial\bar{u}}{\partial x}] \\ \frac{\partial\tilde{\rho}}{\partial t} + \bar{v}\frac{\partial\tilde{\rho}}{\partial y} + \bar{\rho}\frac{\partial\tilde{v}}{\partial y} + \left[\tilde{v}\frac{\partial(\bar{\rho}+\tilde{\rho})}{\partial y} + \tilde{\rho}\frac{\partial(\bar{v}+\tilde{v})}{\partial y}\right] = -[\frac{\partial\bar{\rho}}{\partial t} + \bar{v}\frac{\partial\bar{\rho}}{\partial y} + \bar{\rho}\frac{\partial\bar{v}}{\partial y}] \end{cases} \tag{3.2.7}$$

and

$$\begin{cases} \frac{\partial\tilde{u}}{\partial t} + \bar{u}\frac{\partial\tilde{v}}{\partial x} + \bar{v}\frac{\partial\tilde{u}}{\partial y} + \frac{1}{\bar{\rho}}\frac{\partial\tilde{P}}{\partial x} - \frac{f_1}{\bar{\rho}} + \left[\frac{\tilde{\rho}}{\bar{\rho}}\frac{\partial(\bar{u}+\tilde{u})}{\partial t} + \left(\tilde{u} + \frac{\tilde{\rho}}{\bar{\rho}}(\bar{u}+\tilde{u})\right)\frac{\partial(\bar{v}+\tilde{v})}{\partial x} + \left(\tilde{v} + \frac{\tilde{\rho}}{\bar{\rho}}(\bar{v}+\tilde{v})\right)\frac{\partial(\bar{u}+\tilde{u})}{\partial y}\right] \\ \qquad = -[\frac{\partial\bar{u}}{\partial t} + \bar{u}\frac{\partial\bar{v}}{\partial x} + \bar{v}\frac{\partial\bar{u}}{\partial y} + \frac{1}{\bar{\rho}}\frac{\partial\bar{P}}{\partial x} - \frac{\bar{f}_1}{\bar{\rho}}] \\ \frac{\partial\tilde{v}}{\partial t} + \bar{v}\frac{\partial\tilde{u}}{\partial y} + \bar{u}\frac{\partial\tilde{v}}{\partial x} + \frac{1}{\bar{\rho}}\frac{\partial\tilde{P}}{\partial y} - \frac{f_2}{\bar{\rho}} + \left[\frac{\tilde{\rho}}{\bar{\rho}}\frac{\partial(\bar{v}+\tilde{v})}{\partial t} + \left(\tilde{v} + \frac{\tilde{\rho}}{\bar{\rho}}(\bar{v}+\tilde{v})\right)\frac{\partial(\bar{u}+\tilde{u})}{\partial y} + \left(\tilde{u} + \frac{\tilde{\rho}}{\bar{\rho}}(\bar{u}+\tilde{u})\right)\frac{\partial(\bar{v}+\tilde{v})}{\partial x}\right] \\ \qquad = -[\frac{\partial\bar{v}}{\partial t} + \bar{v}\frac{\partial\bar{u}}{\partial y} + \bar{u}\frac{\partial\bar{v}}{\partial x} + \frac{1}{\bar{\rho}}\frac{\partial\bar{P}}{\partial y} - \frac{\bar{f}_2}{\bar{\rho}}] \end{cases} \tag{3.2.8}$$

It can be seen that (3.2.8) may be written in the form of (3.2.6) where

$$E\{\bar{u}\}\tilde{u} = \begin{cases} \begin{bmatrix} \frac{\partial\tilde{\rho}}{\partial t} + \bar{u}\frac{\partial\tilde{\rho}}{\partial x} + \bar{\rho}\frac{\partial\tilde{u}}{\partial x} \\ \frac{\partial\tilde{u}}{\partial t} + \bar{u}\frac{\partial\tilde{v}}{\partial x} + \bar{v}\frac{\partial\tilde{u}}{\partial y} + \frac{1}{\bar{\rho}}\frac{\partial\tilde{P}}{\partial x} - \frac{\widetilde{f_1}}{\bar{\rho}} \end{bmatrix} \\ \begin{bmatrix} \frac{\partial\tilde{\rho}}{\partial t} + \bar{v}\frac{\partial\tilde{\rho}}{\partial y} + \bar{\rho}\frac{\partial\tilde{v}}{\partial y} \\ \frac{\partial\tilde{v}}{\partial t} + \bar{v}\frac{\partial\tilde{u}}{\partial y} + \bar{u}\frac{\partial\tilde{v}}{\partial x} + \frac{1}{\bar{\rho}}\frac{\partial\tilde{P}}{\partial y} - \frac{\widetilde{f_2}}{\bar{\rho}} \end{bmatrix} \end{cases}, \tag{3.2.9}$$

$$K[\bar{u},\tilde{u}] = \begin{cases} \begin{bmatrix} \tilde{u}\frac{\partial(\bar{\rho}+\tilde{\rho})}{\partial x} + \tilde{\rho}\frac{\partial(\bar{u}+\tilde{u})}{\partial x} \\ \frac{\tilde{\rho}}{\bar{\rho}}\frac{\partial(\bar{u}+\tilde{u})}{\partial t} + \left(\tilde{u} + \frac{\tilde{\rho}}{\bar{\rho}}(\bar{u}+\tilde{u})\right)\frac{\partial(\bar{v}+\tilde{v})}{\partial x} + \left(\tilde{v} + \frac{\tilde{\rho}}{\bar{\rho}}(\bar{v}+\tilde{v})\right)\frac{\partial(\bar{u}+\tilde{u})}{\partial y} \end{bmatrix} \\ \begin{bmatrix} \tilde{v}\frac{\partial(\bar{\rho}+\tilde{\rho})}{\partial y} + \tilde{\rho}\frac{\partial(\bar{v}+\tilde{v})}{\partial y} \\ \frac{\tilde{\rho}}{\bar{\rho}}\frac{\partial(\bar{v}+\tilde{v})}{\partial t} + \left(\tilde{v} + \frac{\tilde{\rho}}{\bar{\rho}}(\bar{v}+\tilde{v})\right)\frac{\partial(\bar{u}+\tilde{u})}{\partial y} + \left(\tilde{u} + \frac{\tilde{\rho}}{\bar{\rho}}(\bar{u}+\tilde{u})\right)\frac{\partial(\bar{v}+\tilde{v})}{\partial x} \end{bmatrix} \end{cases} \tag{3.2.10}$$

$$R = \begin{Bmatrix} \begin{bmatrix} -[\frac{\partial \bar{\rho}}{\partial t} + \bar{u}\frac{\partial \bar{\rho}}{\partial x} + \bar{\rho}\frac{\partial \bar{u}}{\partial x}] \\ -[\frac{\partial \bar{u}}{\partial t} + \bar{u}\frac{\partial \bar{v}}{\partial x} + \bar{v}\frac{\partial \bar{u}}{\partial y} + \frac{1}{\bar{\rho}}\frac{\partial \bar{P}}{\partial x} - \frac{\bar{f}_1}{\bar{\rho}}] \end{bmatrix} \\ \begin{bmatrix} -[\frac{\partial \bar{\rho}}{\partial t} + \bar{v}\frac{\partial \bar{\rho}}{\partial y} + \bar{\rho}\frac{\partial \bar{v}}{\partial y}] \\ -[\frac{\partial \bar{v}}{\partial t} + \bar{v}\frac{\partial \bar{u}}{\partial y} + \bar{u}\frac{\partial \bar{v}}{\partial x} + \frac{1}{\bar{\rho}}\frac{\partial \bar{P}}{\partial y} - \frac{\bar{f}_2}{\bar{\rho}}] \end{bmatrix} \end{Bmatrix} \equiv f - L(\bar{U}). \qquad (3.2.11)$$

The defect correction framework for a 2-scale problem in Navier-Stokes equation is now listed as below:

Step 1:

Solve $L(\bar{U}) = f$ using a CFD package simulating LES or RANS.

Step 2:

Compute defect $R = L(\bar{U} + \tilde{U}) - L(\bar{U})$.

Step 3:

Solve the defect correction problem/simplified problem $E\{\bar{u}\}\tilde{u} + K[\bar{u}, \tilde{u}] = R$.

Step 4:

Correct the approximation $U = \bar{U} + \tilde{U}$.

From the knowledge of physics of fluids, the acoustic perturbations $\tilde{\rho}$, $\tilde{u}$ and $\tilde{v}$ are of very small magnitude (this is not true for their derivatives), therefore, K may be considered negligible due to the reason that any feedback from the propagation waves to the flow can be completely ignored. Hence the equation $E\{\bar{u}\}u = R$, with E given by (3.2.9), which is known as the linearized Euler equation, can be solved in an easier way. The remaining question is to obtain the approximate solution $\bar{U}$ to the original problem (3.2.4). It is well known that CFD analysis packages provide excellent methods for the solution of $L(\bar{U}) = f$. Therefore one requires to use a Reynolds averaged Navier-Stokes package supplemented with turbulence models to provide a solution of $\bar{U}$. Physically, one requires $\bar{U}$ to be as accurate as possible to capture all the physics such as turbulence and vortices.

3.3 DCM for Large Eddy Simulation

As mentioned in the previous chapter, Large Eddy Simulation is one of the common numerical techniques used to solve the PDE governing turbulent fluid flow. Within the technique, the large scale motions of the flow are calculated, while the effect of the smaller scales are modelled using a sub-grid scale model. Let's recall the Navier-Stokes equations for an incompressible fluid,

$$\frac{\partial u_i}{\partial t} + \frac{\partial u_i u_j}{\partial x_j} + \frac{1}{\rho}\frac{\partial p}{\partial x_i} - \nu \frac{\partial^2 u_i}{\partial x_i \partial x_j} = 0 \tag{3.3.1}$$

Decompose each variable such as $u_i = \bar{u}_i + \tilde{u}_i$ where $\bar{u}_i$ represents the variable in the average mean flow and $\tilde{u}_i$ is the variable perturbation that is in several magnitudes smaller than the average mean flow. Therefore (3.3.1) becomes

$$\frac{\partial(\bar{u}_i + \tilde{u}_i)}{\partial t} + \frac{\partial(\bar{u}_i + \tilde{u}_i)(\bar{u}_j + \tilde{u}_j)}{\partial x_j} + \frac{1}{\rho}\frac{\partial(\bar{p} + \tilde{p})}{\partial x_i} - \nu \frac{\partial^2(\bar{u}_i + \tilde{u}_i)}{\partial x_i \partial x_j} = 0. \tag{3.3.2}$$

Hence

$$\frac{\partial \bar{u}_i}{\partial t} + \frac{\partial \bar{u}_i \bar{u}_j}{\partial x_j} + \frac{1}{\rho}\frac{\partial \bar{p}}{\partial x_i} - \nu \frac{\partial^2 \bar{u}_i}{\partial x_i \partial x_j} + \left(\frac{\partial \tilde{u}_i}{\partial t} + \frac{\partial \bar{u}_i \tilde{u}_j}{\partial x_j} + \frac{\partial \tilde{u}_i \bar{u}_j}{\partial x_j} + \frac{1}{\rho}\frac{\partial \tilde{p}}{\partial x_i} - \nu \frac{\partial^2 \tilde{u}_i}{\partial x_i \partial x_j} \right) = 0, \tag{3.3.3}$$

assuming $\frac{\partial \tilde{u}_i \tilde{u}_j}{\partial x_j}$ is negligible.

In the case of LES, all perturbation terms (in bracket) in (3.3.3) is denoted as τ in Equation (2.5) and such term will not be calculated using CFD techniques but instead of being modelled by SGS modelling. The objective here is to directly calculate the perturbation terms incorporating with the use of DCM.

The average mean flow terms can be estimated using a CFD solver by eliminating all perturbation terms from (3.3.3), i.e. assuming

$$\frac{\partial \bar{u}_i}{\partial t} + \frac{\partial \bar{u}_i \bar{u}_j}{\partial x_j} + \frac{1}{\rho}\frac{\partial \bar{p}}{\partial x_i} - \nu \frac{\partial^2 \bar{u}_i}{\partial x_i \partial x_j} = 0 \tag{3.3.4}$$

to solve for an approximation of the mean flow terms. The residual hence becomes the difference between (3.3.3) and (3.3.4)

$$r := \frac{\partial \tilde{u}_i}{\partial t} + \frac{\partial \tilde{U}_{ij}}{\partial x_j} + \frac{1}{\rho}\frac{\partial \tilde{p}}{\partial x_i} - \nu \frac{\partial^2 \tilde{u}_i}{\partial x_i \partial x_j} = 0, \tag{3.3.5}$$

where $\frac{\partial \widetilde{U}_{ij}}{\partial x_j} = \frac{\partial \overline{u}_i \widetilde{u}_j}{\partial x_j} + \frac{\partial \widetilde{u}_i \overline{u}_j}{\partial x_j}$.

Comparing the perturbation term here with the similar term in the LES model, there is a clear difference between the two. In LES, all perturbation terms are pre-modelled using SGS modelling whereas here they can be derived directly using the existing CFD solver as a correction term when solving the mean flow components.

Subsequently it is also important to note that the average mean flow term $\overline{u}_i$ used here is different from the $\overline{u}_i$ in LES method mentioned in the previous chapter. $\overline{u}_{i\_LES}$ is calculated using the modelled result τ by SGS model, whereas the $\overline{u}_i$ here is the direct calculation from a CFD solver. The advantages here are (1) the avoidance of using any modelling tools and (2) an improvement on sufficient use of existing techniques without changing the structure of the calculation matrix of a CFD solver.

3.4 DCM for Lighthill's Acoustic Analogy

Also briefly mentioned in the previous chapter, Lighthill essentially recast the governing equations of fluid motion in the form of an inhomogeneous wave equation suitable to be applied in the far-field. Consider the flow of a compressible, viscous fluid in the absence of applied body forces. A complete set of equations which govern its motion is given by

Conservation of Mass

$$\frac{\partial \rho}{\partial t} + \frac{\partial (\rho u_i)}{\partial x_i} = 0. \tag{3.4.1}$$

Conservation of Momentum

$$\frac{\partial (\rho u_i)}{\partial t} + \frac{\partial (\rho u_i u_j + p_{ij})}{\partial x_j} = 0, \tag{3.4.2}$$

where ρ and p are the density and pressure of the fluid respectively, u_i is the velocity components in the coordinate directions x_i and t is the time.

Assuming the flow is taking place in a fluid with a constant density $\bar{\rho}$, a sufficient set of equations of motion then becomes:

Conservation of Mass

$$\frac{\partial \bar{\rho}}{\partial t} + \frac{\partial (\bar{\rho}\bar{u}_i)}{\partial x_i} = 0. \tag{3.4.3}$$

Conservation of Momentum

$$\bar{\rho}\frac{\partial \bar{u}_i}{\partial t} + \frac{\partial \left(\bar{\rho}\bar{u}_i\bar{u}_j + \bar{p}_{ij}\right)}{\partial x_j} = 0, \tag{3.4.4}$$

where $\bar{p}$ and $\bar{u}_i$ are the pressure and velocity components, respectively, in the incompressible flow.

Consider now the solution of the compressible flow governed by (3.4.1) and (3.4.2). Let

$$\begin{aligned} u_i &= \bar{u}_i + \tilde{u}_i \\ p &= \bar{p} + \tilde{p} \\ \rho &= \bar{\rho} + \tilde{\rho} \end{aligned} \tag{3.4.5}$$

where $\tilde{u}_i$, $\tilde{p}$ and $\tilde{\rho}$ are the fluctuations in the velocity components, pressure about their compressible counterparts and the fluctuation of the density.

Employing the expansions (3.4.5) in (3.4.1) and (3.4.2),

Conservation of Mass

$$\frac{\partial (\bar{\rho}+\tilde{\rho})}{\partial t} + \frac{\partial \left((\bar{\rho}+\tilde{\rho})(\bar{u}_i+\tilde{u}_i)\right)}{\partial x_i} = 0, \tag{3.4.6}$$

Conservation of Momentum

$$\frac{\partial \left((\bar{\rho}+\tilde{\rho})(\bar{u}_i+\tilde{u}_i)\right)}{\partial t} + \frac{\partial \left((\bar{\rho}+\tilde{\rho})(\bar{u}_i+\tilde{u}_i)(\bar{u}_j+\tilde{u}_j)+(\bar{p}_{ij}+\tilde{p}_{ij})\right)}{\partial x_j} = 0. \tag{3.4.7}$$

Hence,

$$\frac{\partial \bar{\rho}}{\partial t} + \frac{\partial (\bar{\rho}\bar{u}_i)}{\partial x_i} + \left(\frac{\partial \tilde{\rho}}{\partial t} + \frac{\partial}{\partial x_i}\left(\widetilde{\rho U_\iota}\right)\right) = 0, \tag{3.4.8}$$

and

$$\bar{\rho}\frac{\partial \bar{u}_i}{\partial t} + \frac{\partial \left(\bar{\rho}\bar{u}_i\bar{u}_j + \bar{p}_{ij}\right)}{\partial x_j} + \left(\frac{\partial}{\partial t}\left(\widetilde{\rho U_\iota}\right) + \frac{\partial}{\partial x_j}\left(\widetilde{\rho U_\iota U_J} + \tilde{p}_{ij}\right)\right) = 0, \tag{3.4.9}$$

where $\widetilde{\rho U_\iota} = \bar{\rho}\tilde{u}_i + \tilde{\rho}(\bar{u}_i + \tilde{u}_i)$ and $\widetilde{\rho U_\iota U_J} = \bar{\rho}\left(\bar{u}_i\tilde{u}_j + \tilde{u}_i\bar{u}_j\right) + \tilde{\rho}\left(\bar{u}_i\bar{u}_j + \bar{u}_i\tilde{u}_j + \tilde{u}_i\bar{u}_j\right)$, assuming $\frac{\partial}{\partial x_i}\left(\tilde{u}_i\tilde{u}_j\right)$ is negligible.

The flow variables in the incompressible flow can be estimated using a CFD solver by solving governing equation (3.4.3) and (3.4.4). The residuals hence become the difference between (3.4.8), (3.4.9) and (3.4.3), (3.4.4)

$$r_{Mass} := \frac{\partial \widetilde{\rho}}{\partial t} + \frac{\partial}{\partial x_i}\left(\widetilde{\rho U_i}\right) = 0, \tag{3.4.10}$$

and

$$r_{Momentum} := \frac{\partial}{\partial t}\left(\widetilde{\rho U_i}\right) + \frac{\partial}{\partial x_j}\left(\widetilde{\rho U_i U_j} + \tilde{p}_{ij}\right) = 0. \tag{3.4.11}$$

Both Lighthill's analogy and the current approach require the flow variables in the incompressible flow to be solved using a CFD solver that resolves the governing equations of fluid motion. However, in the context of the difference beyond this point in process, in Lighthill's wave equation (2.17), one has to develop a separate solver to resolve the source term on its right hand side in order to obtain the fluctuation of the flow's compressible counterparts; whereas here such flow's compressible variables can be derived directly using the same CFD solver as a correction term when solving the incompressible flow components.

And, in this example again, it demonstrates the advantage of the defect correction approach being an improvement on sufficient use of existing techniques without changing the structure of the calculation matrix of an existing CFD solver.

3.5 Closure

This chapter has set a framework of the DCM for problems that exhibit multiple scales at the continuum level. Especially, this is linked to problems in CFD and CAA. The most advantage of employing DCM in these problems is the sufficient use of existing software calculation matrix structure.

An application to aeroacoustic noise analysis will be detailed in the next chapter and this will lead to the idea of software automation utilizing defect correction concept.

Chapter 4 APPLICATIONS TO AEROACOUSTIC NOISE ANALYSIS

In automotive industry, aerodynamic noise is the noise caused by temporal fluctuations of airflow around the body of a moving automobile. Aerodynamically induced noise represents a significant contribution to noise pollution inside passenger compartment. This aerodynamics noise becomes more intense as the velocity of the flow increases.

A significant contribution to interior noise in road vehicles is buffeting due to the aerodynamic flow over an open sunroof. Buffeting noise is characterized by low frequency (often 10 to 50 Hz) tonal noise of substantial magnitude and may be a truly exhausting and even hazardous experience if persisting over long periods. The origin of buffeting noise is a shear-layer instability forming in the opening of a cavity subjected to grazing flow. In the shear-layer vortices are produced and they travel downstream of the opening, eventually hitting the rear edge. When the vortex breaks, a pressure wave which enters into the cavity is produced. At a certain speed, the vortex shedding frequency in the shear layer will match an acoustic mode of the cavity. Often, as in many wind instruments (e.g. the flute), the resonance is in the form of a standing wave. For an automobile cavity, the resonance is in the form of a Helmholtz mode, a special case of a standing wave but with a distinctly lower frequency. This is the same sound generation mechanism as when blowing air over a bottle opening. The reason for the high amplitudes is partly the fact that the listeners (driver and passengers) are located within the resonant body itself.

4.1 An overview of Techniques Used for Sunroof Buffeting Noise Problems

4.1.1 Lattice Boltzmann Method

Lattice Boltzmann Method (LBM) is a lattice-based system built upon a mathematical approach. LBM is a discrete formulation of the Boltzmann kinetic theory. The general form of the Boltzmann kinetic equation is

$$\frac{\partial f}{\partial t} + c \cdot \nabla f = \Omega(f), \tag{4.1.1.1}$$

where function $f(x,c,t)$ represents the number of particles whose positions and velocities are x and c at time t. $\Omega(f)$ is an explicit expression for the collision function which determines physics of the flow. However, the macroscopic variables such as density ρ, velocity u and internal energy e can be deduced without knowing the form of $\Omega(f)$.

Due to the quadratic aspect of $\Omega(f)$ and the multiple integrations in its analytical formulation, a linearized collision operator with a single relaxation time τ has chosen to present the collision operator $\Omega(f)$

$$\Omega = -\frac{f - f^{(eq)}}{\tau}, \tag{4.1.1.2}$$

where $f^{(eq)}$ is the equilibrium function.

Coupling between vortex shedding over automotive sunroof and acoustic resonance of the passenger compartment can induce strong self-sustained oscillations of the flow. A detailed study of the phenomenon by Ricot, Maillard and Bailly [Ricot et al, 2001] shows that aerodynamic coupling also participated to the self-sustained oscillation when the flow characteristics lead to aerodynamic frequencies outside the "frequency-of-aerodynamic-instability and resonance-frequency-of-vehicle matching range", which is when the maximum amplitude oscillation occurs. LBM is used. Instead of solving the Navier-Stokes equations, the discrete Boltzmann equation is solved to simulate the flow of Newtonian fluid with collision models such as Bhatnagar-Gross-Krook (BGK). Unlike conventional numerical codes which use a discretisation of macroscopic continuum

equations such as the Navier-Stokes equations, the LBM is based on mesoscopic kinetic equations and a particle distribution function.

A benchmark case has been chosen to study the possibility of performing turbulent simulations with the solver. A free shear layer expands from a splitter plate between two parallel flows with an impingement wedge placed at downstream (see Figure 4.1). A modelling of the effects of sub-grid turbulent fluctuations is introduced. A structured, cubic Cartesian mesh and a grid refinement scheme which refines the grid size in each direction equally and successively by a factor two is applied.

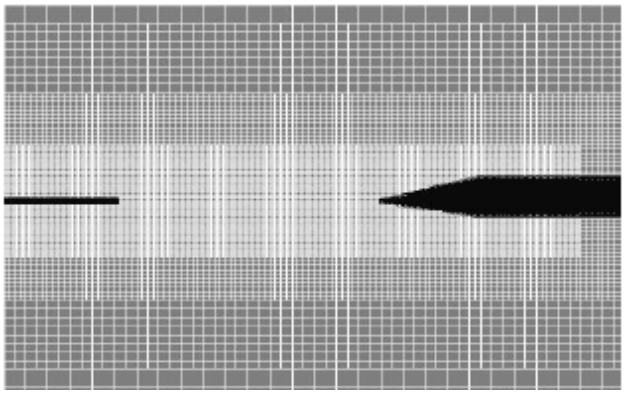

Figure 4.1: A benchmark case: splitter plate (left) and impingement wedge (right)

Velocity signals show that the amplitude of aerodynamic disturbances is too weak compared to experimental data. This default is due to the damping effect of the eddy viscosity model based on the $k-\varepsilon$ RNG equations. Because of the over-damping of high frequency fluctuations, the preferred oscillation frequency is shifted toward a lower spurious resonance frequency of the computational domain. The turbulence modelling is still a limiting aspect of flow simulations with Lattice Boltzmann Method.

4.1.2 Large Eddy Simulation (Two Dimensional)

As mentioned in the introduction, direct sound computation based on LES for application to engineering flows still remains expensive due to the requirement of an accurate three-dimensional computation with fine mesh and small time-steps plus other computational issues. Dubsky [Dubsky, 2003] tries to investigate the possibilities and restrictions of

LES for solving the aeroacoustic properties for a model of car sunroof. A simplified model of the sunroof type is used.

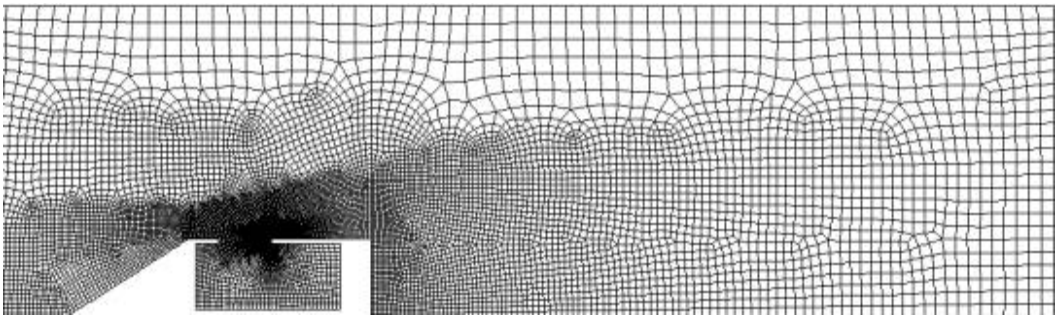

Figure 4.2: A simplified model of the sunroof and car cavity

The flow can be treated as incompressible, as the compressibility has no effect on the acoustics according to Ffowcs-Williams [Ffowcs–William, 1969]. Central differencing scheme for momentum is chosen.

The time step is tuned in each resolution regions to ensure a constant CFL < 1. CFL condition: Courant number is a relation between the time step size, velocity of the flow and the cell size. The appropriate time step size can be calculated from Equation 4.1.2.1 to satisfy the condition $C < 1$.

$$\delta t = C\frac{\delta x}{u}. \tag{4.1.2.1}$$

C is the Courant number, δt is the size of the time step, u is the highest velocity component and δx stands for the cell size in direction of u. The size of the time step is related to the highest frequency (20 kHz), which can be registered by human ear, i.e. $\delta t << t = \frac{1}{f} = \frac{1}{20000} = 5e^{-5}s$. Breaking this condition set would not be able to analyse the whole spectrum of audible sound. However, to make the simulation faster, it is possible to go slightly over these restrictions, as this limitation is based on the highest frequency (“worst” scenario).

Strouhal number is used to check the obtained frequency from the noise analysis with the empiric formula result.

$$Str = \frac{fd}{U_0} = 0.198\left(1 - \frac{19.7}{\mathrm{Re}}\right). \qquad (4.1.2.1)$$

Three assumptions for noise analysis:

1. The sound is radiated into free space.
2. The sound induced by fluid flow is weak (i.e. the backward-interaction of acoustic phenomena on the fluid flow is negligible).
3. The fluid flow is not sensitive to the sound induced by the fluid flow.

To reach the dynamically steady state, Dubsky used Reynolds Stress turbulence model and steady simulation with default settings to reach a state close to the dynamically steady one. This reduces the calculation time significantly. Monitoring pressure in certain point and analysing its behaviour should identify the dynamically steady state.

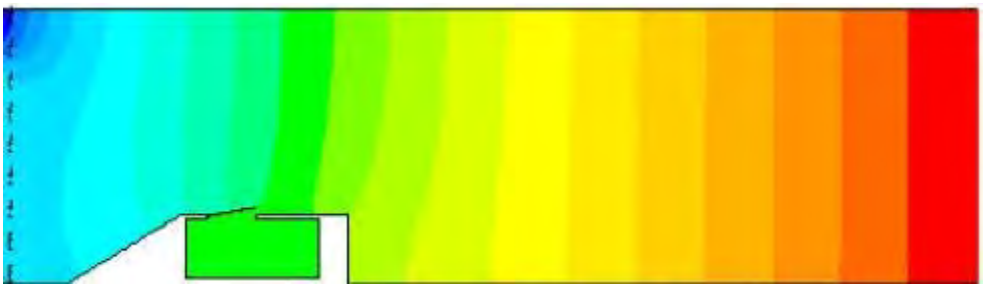

Figure 4.3: Static Pressure Contours – LES

Figure 4.4: Static Pressure Contours – steady state, RSM

In this sunroof problem, the LES simulation failed to converge, which also caused the noise analysis result not realistic. The reason for the incorrect results may be caused by:

• Mesh properties. The size difference between the small cells near the sunroof tip and the bigger ones near the boundaries of the domain is simply too large. This makes large differences in the sub grid turbulence modelling. The value of sub grid turbulent viscosity varies too much across the domain.

• Using of the paved meshing method. It works on simple geometries (e.g. the cylinder problem). Unfortunately, for more complicated geometries the benefits of using mapped quadrilateral cells are either too small or it is not possible at all to build some reasonable mesh.

• The use of LES in 2D. Because the turbulence is phenomenon occurring in 3D

Because of extreme time and computational power needed, it turned out (as expected) that it was not possible to solve the acoustics of the example of the car geometry by direct sound computation based on LES, even if it was simplified and modelled in 2D.

4.1.3 Incompressible Navier-Stokes Equations plus Weak Compressible Flow Model

Use the finite volume method (FVM) on the collocated grid system to conserve the mass and the momentum on the discretized fundamental equations. The weak compressible flow model derived through the assumption of a slight nominal density fluctuation is used to simulate the buffeting phenomenon by Inagaki, Murata, Kondoh and Abe [Inagaki et al, 2002].

When conducting actual aerodynamic noise analysis, two methods can be applied after accurately calculating the fluctuations at the flow field that is the source of the noise:

a) The characteristics of noise are indirectly predicted utilizing the flow pressure fluctuations.

b) The sound pressure at the point of observation is calculated by applying the Lighthill-Curle theory to the computational results of the unsteady flow field.

For ordinary flow velocity of a vehicle in motion, the airflow around the vehicle body is treated as an incompressible flow, which allows changes in density to be ignored. However, in regards to buffeting noise analysis, the treatment of incompressible flow is inadequate.

The governing equations for dimensionless unsteady incompressible flow can be expressed as

$$\frac{\partial u_j}{\partial x_j} = 0 \tag{4.1.3.1}$$

and

$$\frac{\partial u_i}{\partial t} + \frac{\partial u_i u_j}{\partial x_j} = -\frac{1}{\rho}\frac{\partial p}{\partial x_i} + \frac{\partial \tau_{ij}}{\partial x_j} \tag{4.1.3.2}$$

where

$$\tau_{ij} = \frac{1}{\mathrm{Re}}\left(\frac{\partial u_i}{\partial x_j} + \frac{\partial u_j}{\partial x_i}\right). \tag{4.1.3.3}$$

Also, the Lighthill-Curle theory determines the sound pressure P_a at any observation point using the following equation

$$P_a = \frac{1}{4\pi c}\frac{x_i}{r^2}\frac{\partial}{\partial t}\int_S n_i P dS \tag{4.1.3.4}$$

.

c is the sound speed, x_i is a component of the positional vector of the observation point, r is the distance to the observation point, and P is the flow pressure on an object surface. If the flow pressure on the object surface is determined at every time using Equation (4.1.3.1) and (4.1.3.2), then it is possible to calculate the sound pressure at an observation point using Equation (4.1.3.4). Equation (4.1.3.4) can be derived from the governing equations for compressible flow by simplifying the equation and assuming the following ideal conditions:

a) Unlimited space, in where the object is included completely.

b) The distance to the observation point is sufficiently larger than the sound wavelength.

c) The distance to the observation point is sufficiently larger than the size of the interior object.

d) Flow velocity is significantly lower than sound speed – low Mach number.

Structured grid is utilized – uniformly lined (orthogonal, equidistant) much like a chessboard at least in the computational space. In each grid cell, physical quantities (velocity, pressure, etc.) are calculated by the discretization of the basic flow equation based on a high-accuracy scheme. Generally, body fitted grid is used, which fits the grid lines on the boundary surface of the target object and concentrates the grid points near the surface. However, when geometries with complicated areas are computed, it is difficult to cover them with single structured grid block of sufficient quality.

To deal with such problem, an overset grid method is introduced which focuses in local shapes on the object and boundary. After generation of a partial grid appropriate for each boundary shape or the characteristics of flow field, multiple grid blocks are layered over each other (so that data can be mutually transferred between the grids in the overlapped region) and the entire area to be computed is covered. This method is extremely effective for reducing man-hours and improving usability, also, computational accuracy is improved as a result of the ability to generate a better grid.

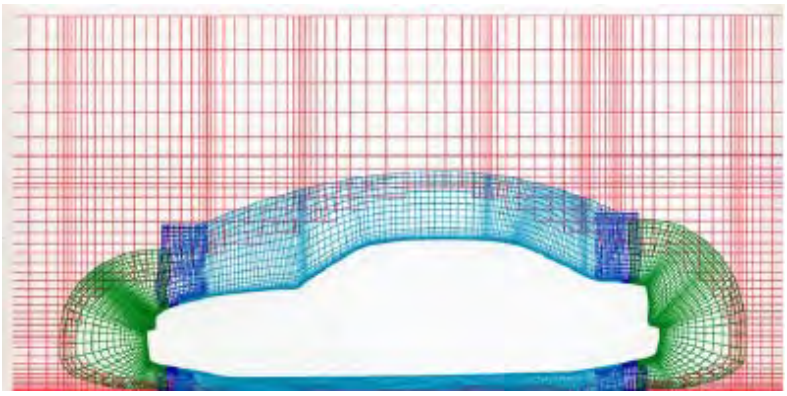

Figure 4.5: An example of overset grid system

For the governing equations, QUICK scheme (the third order upwind difference scheme) is applied, and the Crank-Nicolson method is used on the time integration.

Because Helmholtz resonance is caused by slight density fluctuations, it is impossible to predict the buffeting noise using a computation that assumes an incompressible flow. Accordingly, the following governing equations, which model the weak compressibility on the flow field of low Mach numbers, are solved numerically.

$$M^2\left\{\frac{\partial p}{\partial t}+u_j\frac{\partial p}{\partial x_j}\right\}+\frac{\partial u_i}{\partial x_j}=0 \qquad (4.1.3.5)$$

$$\frac{\partial u_i}{\partial t}+\frac{\partial u_i u_j}{\partial x_j}-u_i\frac{\partial u_j}{\partial x_j}=-\frac{1}{\rho}\frac{\partial p}{\partial x_i}+\frac{\partial \tau_{ij}}{\partial x_j} \qquad (4.1.3.6)$$

M is the Mach number and has a value of approximately 0.1 at the flow around the vehicle body. The equations of the weak compressible flow are considered as the incompressible flow Equations (4.1.3.1) and (4.1.3.2) with additional terms. In particular, the left side of the Equation (4.1.3.5) of continuity expresses the effect of weak compressibility. Because the values are small, and also in order to accurately estimate the effects numerically, a method for accurately solving the original Equation (4.1.3.1) of continuity is necessary.

Concerning the estimation of sound pressure fluctuations, Lighthill-Curle theory is thought to be the most reliable, but its field of application is limited. In such cases, it is necessary to use the pressure fluctuations of the flow field as a substitute.

4.2 The Present Approach – The Current Study

In the last section, various techniques used by different researchers in the last decade to simulate buffeting phenomenon due to an opening sunroof of an automobile have been reviewed. The latest industrial practice, which is currently used by a number of major automobile manufacturers, involves the use of PowerFLOW [Exa Corporation], a commercial code which employs the Lattice Boltzmann Method (LBM) to recover the Navier-Stokes equations. The resolved time history of pressure fluctuation under the sunroof could then be converted into the frequency domain by PowerACOUSTICS [Exa Corporation], a code to test the acoustic (Helmholtz) resonance frequency of the cabin. The downside of such approach is the computational cost. For a typical sunroof simulation, on average it requires approximately 10,000 CPU hours. Also, it has been noticed that there has been an improving trendof computational methods from LBM with a $k-\varepsilon$ RNG turbulence model to Subgrid-scale (SGS) turbulence model used in Large Eddy Simulation (LES) and even Direct Numerical Simulation (DNS) can be noticed.

The rapid advance of computational power in recent years allows LES being used on many applications with reasonably high Reynolds number. The main advantage of LES

over those computationally less expensive methods such as Reynolds-averaged Navier-Stokes equations (RANS) is the increased level of detail it can deliver. While RANS methods provide "averaged" results and turbulence models over-damping the high frequency fluctuations, LES is able to predict instantaneous flow characteristics and resolve turbulent flow structures of large scales (i.e. the energy-containing eddies), which are known to contribute most to the sound generation in many problems. Thus it offers significantly more accurate results over RANS for flows involving flow separation or acoustic prediction. LES is used extensively to elucidate the physics of turbulence and to compute flows of industrial relevance, wherever Reynolds-averaged models are not sufficiently accurate and Direct Numerical Simulation techniques are prohibitively expensive.

The difficulty in achieving predictive simulations is perhaps best illustrated by the wide range of approaches that have been developed and are still being used by the turbulence modelling community; Implicit Large Eddy Simulation (ILES) is one of them. ILES is a relatively new approach that combines generality and computational efficiency with documented success in many areas of complex fluid flow. Instead of using a subgrid-scale model for a classic LES to model the motion of those non-energy-contained eddies, ILES uses a higher-order discretisation method with a limiter. The limiter is originally meant to avoid numerical oscillations in the solution, but it also works as a subgrid model for small eddies according to Ciardi, Sagaut, Klein and Dawes [Ciardi et al, 2005]. The concept of using a higher-order discretisation method as a subgrid scale model in ILES, with a fine mesh, small time-steps numerical approach to resolve the unsteady flow field is implemented in this current study described below.

In this current study, a hypothetical car configuration with an open sunroof with part of the compartment forming the resulting cavity has been examined. The car is travelling at a cruising speed with induced flow fluctuation due to the open sunroof. The pressure perturbation along the sunroof is computed by solving the two dimensional unsteady compressible Navier-Stokes equations using a typical commercial Finite Volume CFD package, PHOENICS [CHAM Limited], and the pressure fluctuation due to the sunroof is extracted and analysed. Various high order numerical schemes are tested and compared to provide a better understanding of their advantages and disadvantages for this application. In order to study the acoustic response inside the car compartment, the acoustic pressure distribution is calculated by solving the Helmholtz equation. Some of

the tests carried out in Wang's work [Wang et al, 2004] was based on a two scale expansion in an investigation of car-door cavity is in essence an early incomplete form of the DCM framework. The coupling of software is thus requested after the decoupling of scale difference as discussed in the solution strategies in Chapter 2. Therefore, without loss of generality it would be easier to demonstrate the sunroof cavity noise problem using a simplified approach of an artificial vortex travelling along with the main stream fluid flow over the cavity in order to illustrate the coupling of two different software packages.

4.2.1 Solutions of unsteady Navier-Stokes Equations

Previous experience of an open cavity with a lip shows induced oscillatory fluctuation of pressure by Wang, Djambazov, Lai and Pericleous [Wang et al, 2007] caused by shear layer separation at the upstream end. This leads to further interests in related problems such as a hypothetical car with an open sunroof as depicted in Figure 4.6. The length of the sunroof is 0.6m and the effective depth of the opening lip (thickness of the sunroof) is 0.05m. The free stream velocity is 25 m/s (approx. 90 km/h). In order to excite the flow to get stronger pressure fluctuation response on top of the sunroof, an artificial sinusoidal vertical-velocity disturbance is used to represent a single vortex generated by vehicle travelling at upstream of this car. The vortex strength is given by $W = W_0 \sin(2\pi at)$, where W_0 = -1.2 m/s and a is a parameter chosen as a constant independent of time. Different frequencies of this upstream vertical-velocity disturbance are applied to generate different acoustic responses on the top of the sunroof.

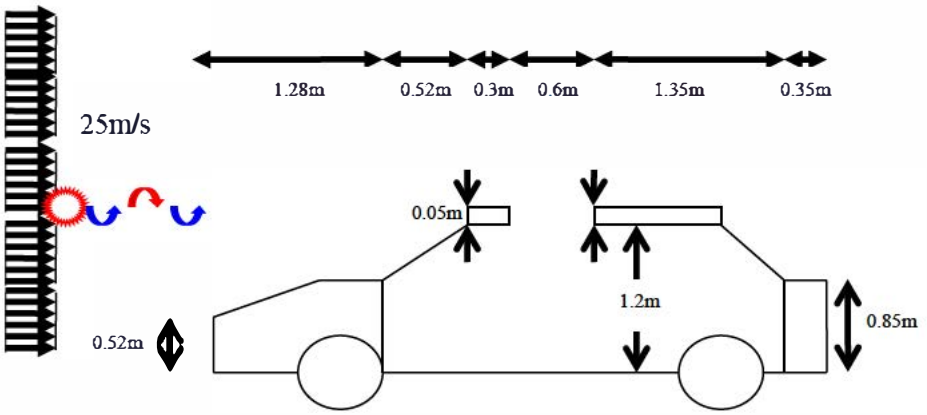

Figure 4.6: A hypothetical car with open sunroof

In this calculation, a Finite Volume based software package, PHOENICS, is used to compute time-accurate unsteady flow fields. The package may be used in the computations of compressible and incompressible flows.

The backflows through the outlet boundary should be avoided. When a strong vortex hits the pressure outlet, it creates backflows which are caused by less well-converged temporal solution (limited by max number of iterations), it affects the vortex shedding from the object. That is why it is necessary to extend the domain downstream. In the present simulation, the computational domain is taken as 17.6m by 8.8m. PHOENICS uses a structured, regular Cartesian mesh and a gird refinement scheme which refines the grid size in each direction equally (see Figure 4.7). The minimum grid size is $\Delta x_{min} = 2.5e^{-2}$m. Four levels of grid resolution are used. To satisfy both the mass and momentum conservation laws, the velocity and pressure field are solved iteratively by using the SIMPLE pressure-correction algorithm proposed by Patankar [Patankar, 1980]. In using PHOENICS, standard boundary conditions are used for inflow, solid wall, and far-field boundaries. Five different discretisation schemes have been tested in this study in order to provide a better understanding of their advantages and disadvantages for the present study. In order to resolve the acoustic disturbance correctly a minimum of 20 temporal integration steps were chosen to represent each oscillation cycle at the highest frequency of interest. The time step length, δt, chosen for the temporal integration is 10^{-3}s resulting in a maximum resolved frequency of 50Hz.

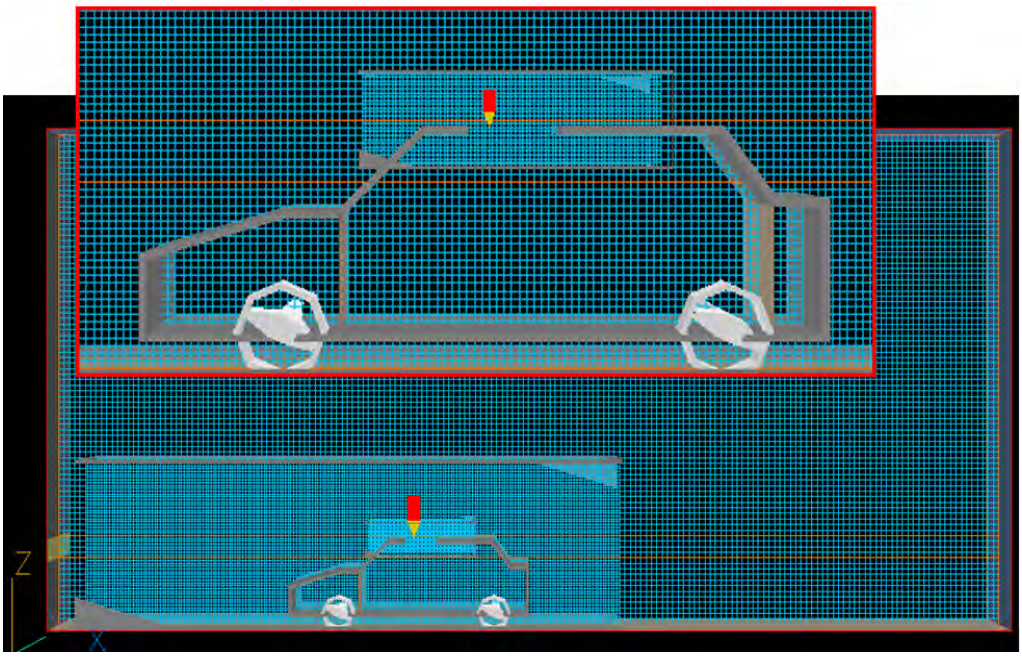

Figure 4.7: Fine Grid applied to the airflow around the car configuration and finer grid specifically focused on top of the sunroof opening

4.2.2 Extracting Pressure Fluctuations

Two factors contributed to the pressure fluctuation above the sunroof. First the incoming flow over certain vehicle's body. Second the artificial disturbance introduced upstream of the configuration. For the present study the artificial disturbance requires a time equal to $528\delta t$ to reach downstream of the sunroof. It is possible to use the pressure obtained from the CFD calculation to examine the frequency response inside the car compartment. The pressure fluctuation along the upper surface of the car configuration and at the sunroof opening is given by $P_f(x,t) = P(x,t) - \overline{P}(x,t)$, where P is the instantaneous pressure distribution along the upper surface obtained by using the CFD calculation and $\overline{P}$ is the background pressure distribution along the upper surface due to the upstream velocity and the car configuration.

4.2.3 Numerical Schemes for Convection Discretisation

In all Finite Volume CFD codes for which cell-centre values of variables are stored, as in the schematic diagram below, values of the variable ϕ are known for the cell centres W,

P and E; but the values of ϕ at face w, which travels from cell W to cell P, or from P to W, may be calculated by using a number of numerical schemes.

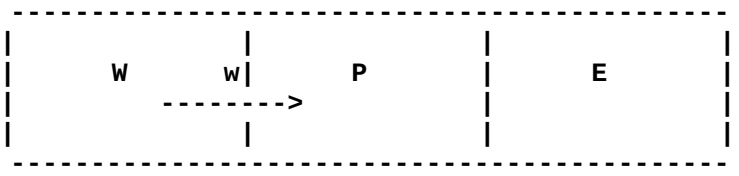

The numerical scheme influences the balance equations for both cell W and cell P. To ensure fairly good solution one can choose $\phi_w = \phi_W$ when the flow is from W to P, but $\phi_w = \phi_P$ when the flow is from P to W. This scheme, or the so-called "hybrid" variant of it, is used as the default numerical scheme, together with other schemes, in PHOENICS. In this study, five different numerical schemes, three linear and two non-linear schemes as listed below, are being tested and each of them has a different approach to calculate the cell face value ϕ_w.

- UDS Upwind-differencing scheme: $\phi_w = \phi_W$
- CDS Central-differencing scheme: $\phi_w = \dfrac{\phi_P + \phi_W}{2}$
- QUICK Quadratic upwind scheme: $\phi_w = \dfrac{3}{8}\phi_P + \dfrac{3}{4}\phi_W - \dfrac{1}{8}\phi_{WW}$
- SMART Bounded QUICK: $\phi_w = \phi_W + 0.5B(\phi_W - \phi_{WW})$
- HQUICK Harmonic QUICK: $\begin{cases} if\ r \le 0, & \phi_w = \phi_W \\ if\ r > 0, & \phi_w = \phi_W + \dfrac{2(\phi_P - \phi_W)(\phi_W - \phi_{WW})}{\phi_P + 2\phi_W - 3\phi_{WW}} \end{cases}$

Here $B = \max\left(0, \min\left(2r, \dfrac{3r+1}{4}, 4\right)\right)$, $r = \dfrac{\phi_P - \phi_W}{\phi_W - \phi_{WW}}$, and ϕ_{WW} is the cell-centre further upstream.

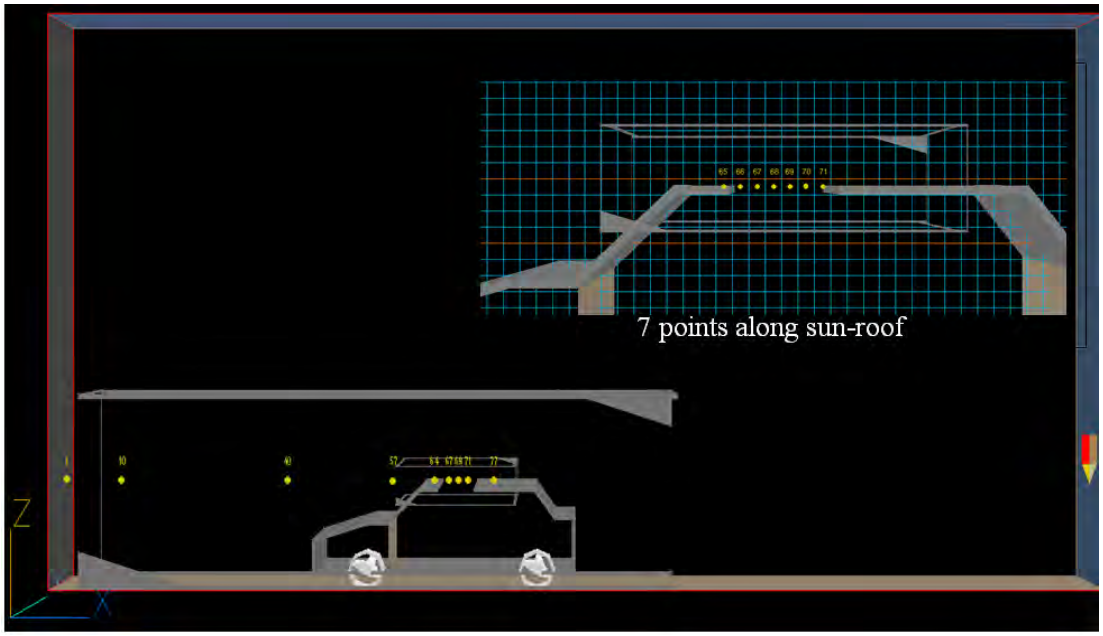

Figure 4.8: Observation points in the computational domain

Figure 4.8 shows nine observation points marked with their location numbers along the same vertical level where the artificial disturbance is introduced. The time history of the pressure fluctuations at these observation points are shown in column 2 in Table 4.1. A zoom-in to the neighbourhood of the sunroof with seven other observation points and their pressure fluctuations are shown in column 3. It can easily be seen that first order accurate Hybrid / Upwind scheme and third order accurate HQUICK scheme are too dissipative to capture any meaningful pressure fluctuation at top of the sunroof and therefore are not suitable for this type of example. As a result, the magnitude of pressure fluctuations observed on top of the sunroof is very small. CDS even failed to converge because the cell Peclet number is not guaranteed to be less than 2. However, SMART and QUICK scheme show more interesting results. The pressure fluctuations on top of the sunroof gradually grow in magnitude in a sinusoidal form. The fluctuations obtained by using QUICK scheme lead to a more stable and regular sinusoidal shape. In a snapshot of vertical velocity disturbance at $t = 0.5s$ (Figure 4.9), it shows the amplitude of aerodynamic disturbances is gradually becoming weaker and weaker. This is due to the numerical scheme dissipation. However, a clear vortex shearing on top the sunroof can still be observed. At this stage, QUICK seems to be the best high order scheme to be applied for this application.

Numerical Scheme	Pressure Fluctuation at nine observing points	Pressure Fluctuation at all seven points on top of sun-roof
Hybrid / Upwind	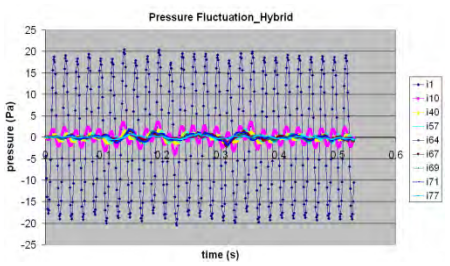	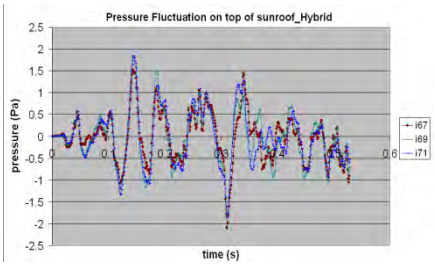
HQUICK	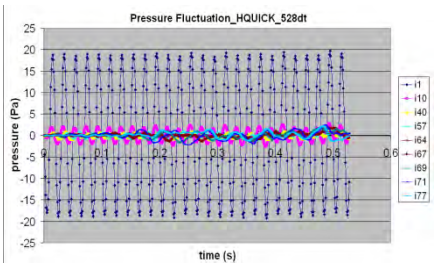	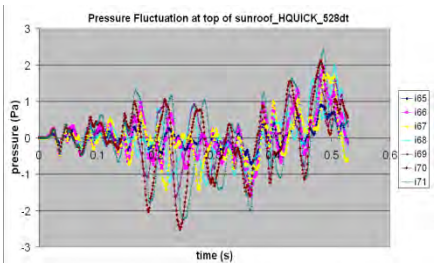
SMART	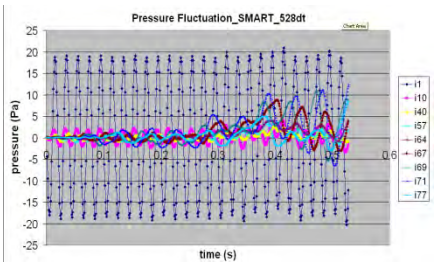	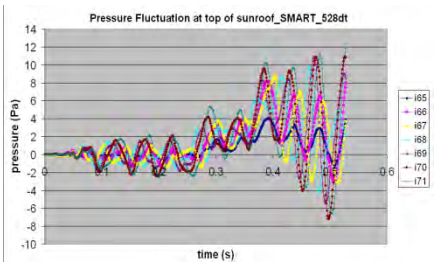
QUICK	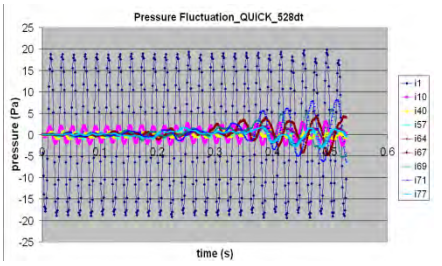	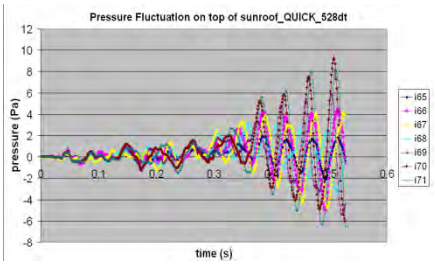

Table 4.1: Comparison of pressure fluctuations using different numerical schemes

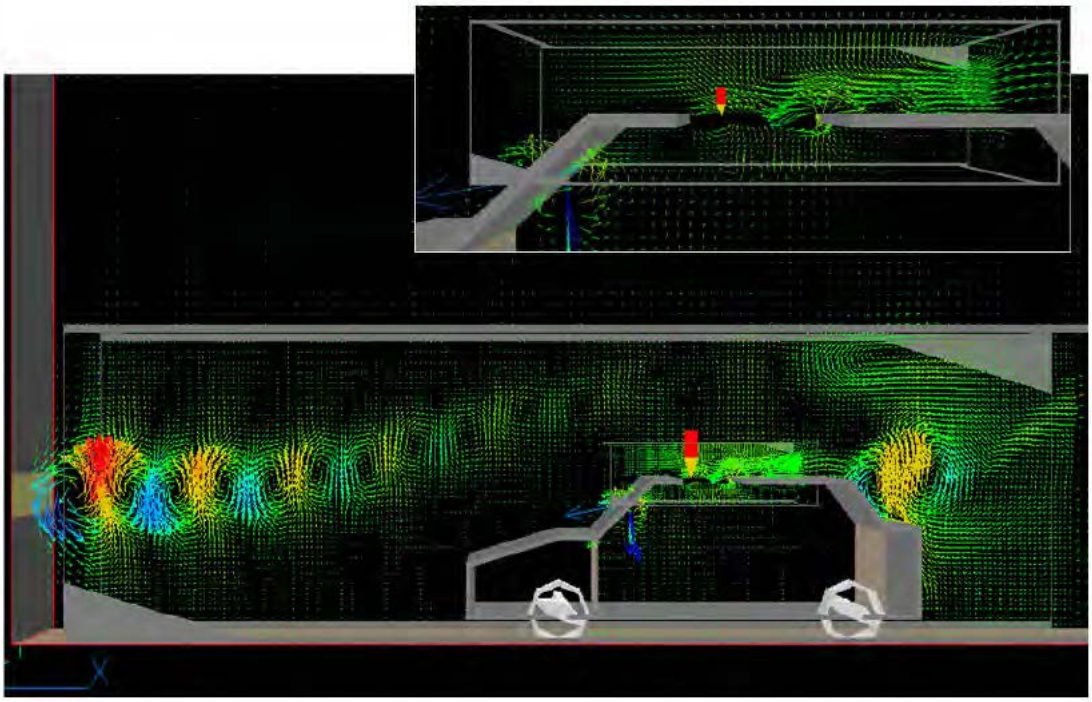

Figure 4.9: A snapshot of Z component velocity disturbance at $t = 0.5s$. On top, it is the zoom-in image on top of the sunroof

4.2.4 Analysis of Acoustic Response

Using the results from the QUICK scheme, frequency components of the pressure fluctuations are then examined by producing an acoustic power spectrum of the time history at all seven points on the sunroof via sampling a 512-point Fast Fourier Transform (FFT). The spectrum is depicted (Figure 4.10) and shows the dominant frequency at all observation points on the sunroof occurs roughly at 13Hz.

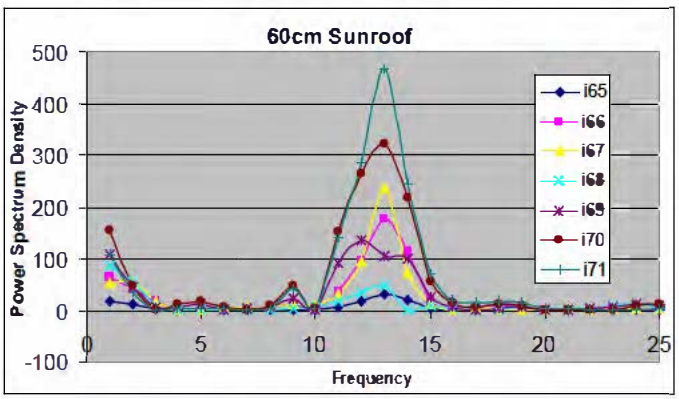

Figure 4.10: Power spectrum density of the time history via a 512-point FFT

The validity of the results of the dominant frequency is checked against a Helmholtz resonator with similar shaped and sized cavity. The resonant frequency for a typical Helmholtz resonator may be approximately calculated by the formula, $f = (c/2\pi)\sqrt{A/(l_{eff}V)}$, where $l_{eff} = l + l_{cor} = l + \eta r$ denotes the effective length of the air at the opening, l is the geometric neck length (i.e. 0.05m, in Figure 4.6). l_{cor} is the end correction on the neck length, which can be expressed by a product of r, the radius of the neck, and η, an empirical coefficient which significantly depends on geometrical configuration and sizes. A is cross sectional area of the neck, V represents the volume of the inside cavity. Although the formula is for an idea situation and completely neglects the shear layer, it gives only an approximate indication of the frequency of oscillation of the cavity. An approximate value of the dominant resonant frequency with $\eta = 16.9$ is around 10.5Hz. It must be pointed out that this is not a strict comparison due to the coefficient unavailable currently for the cavity of the car compartment considered. However, even so, this crude comparison shows that the dominant frequency value obtained through the unsteady computation is a physically acceptable approximation.

To study the acoustic response along the sunroof, different frequencies of the upstream disturbance are applied. Numerical tests as a function of input disturbance are performed to verify the hypothesis that the lower the frequency of disturbance, the lower the frequency of acoustic response obtained. In this study, 25Hz and 10Hz disturbance frequencies are compared with the maximum resolvable frequency of 50Hz (see Table 4.2). The power spectra show that for incoming disturbance at a frequency higher than 25Hz the dominant mode of the noise generated due to the sunroof occurs at roughly 13 Hz which is the resonant frequency. On the other hand for incoming disturbance at lower frequency, say 10 Hz, seems to excite a half harmonic at around 6Hz while maintaining the harmonic of 13Hz at a weaker strength.

50Hz	25Hz	10Hz
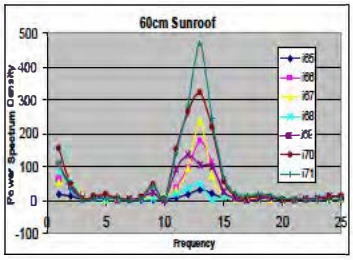	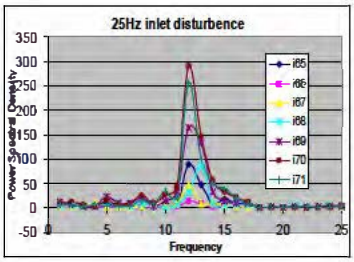	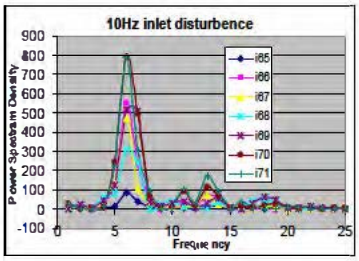
Obtained f = 13Hz	Obtained f = 12Hz	Obtained f = 6Hz

Table 4.2: Comparison of peak frequencies obtained via a 512-point FFT due to different incoming disturbances of 50, 25 and 10Hz

4.2.5 Use of Wave Equation Inside Car Compartment

As mentioned previously, sound waves are typically several orders of magnitude smaller than the pressure variations in the flow filed that account for flow acceleration. The idea of applying DCM comes into the evaluation of the defect due to the pressure produced by the mean flow in such a way that the pressure fluctuation due to the acoustic perturbation is significantly smaller in magnitude, resulting in the decouple of the two disparate magnitudes. The solutions of the Reynolds averaged Navier-Stokes equations (i.e. the solution derived from the existing CFD software, PHOENICS) reveal only a truncated part of the full physical quantities. The basic principle of the defect correction can be applied to recover the propagating acoustic perturbation. By doing so, it relies on Lighthill's acoustic analogy to perform wave travelling.

In Lighthill's acoustic analogy Equation (2.17), the source term on the right hand side of the equation consists detailed fluid flow motion around acoustic source region (near-field). In this particular case, due to the ratio between the width of the opening of the cavity (i.e. sunroof, in this case) and the depth of the cavity (i.e. height inside car compartment) is relatively high; the aerodynamic motion inside the car compartment can be effectively neglected. In other words, Lighthill's equation can be rewritten as a homogeneous wave equation expressed as

$$\frac{\partial^2 \tilde{\rho}}{\partial t^2} - c^2 \nabla^2 \tilde{\rho} = 0. \qquad (4.2.5.1)$$

In order to transfer the wave equation from a time domain into frequency domain, one needs to integrate Equation (4.2.5.1) with respect to time by using Fast Fourier Transform (FFT),

$$\int_{-\infty}^{\infty} \frac{\partial^2 \tilde{\rho}}{\partial t^2} e^{i\omega t} dt - c^2 \int_{-\infty}^{\infty} \nabla^2 \tilde{\rho} e^{i\omega t} dt = 0 \tag{4.2.5.2}$$

one obtains in a simplified form, i.e. Helmholtz equation,

$$-\omega^2 \psi - c^2 \nabla^2 \psi = 0, \tag{4.2.5.3}$$

where

$$\psi = \int_{-\infty}^{\infty} \tilde{\rho} e^{i\omega t} dt \tag{4.2.5.4}$$

.

To implement the acoustic propagation by Helmholtz equation in this case, it is assumed that the flow inside the car compartment is negligible. For the present study the analysis of sound distribution for the dominant frequency of f = 13Hz due to an incoming disturbance of 50 Hz is examined. The power spectrum density along the sunroof is used as Dirichlet boundary conditions for the Helmholtz equation, which calculates the acoustic pressure distribution inside the car compartment.

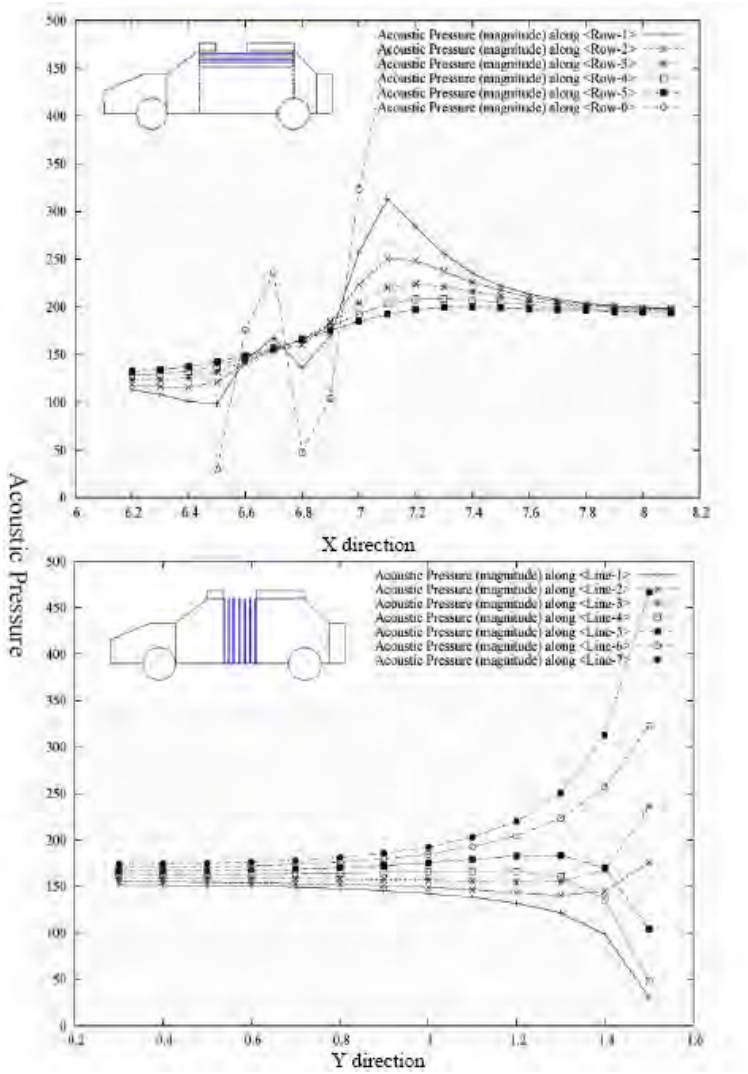

Figure 4.11: Acoustic pressure inside the car component along several horizontal and vertical lines

Figure 4.11 shows the acoustic pressure distribution along several horizontal lines and vertical lines below the sun-roof inside the car compartment. It shows that the highest acoustic pressure is experienced at x 7.1m. On the other hand along the horizontal line just below the sun-roof the pressure shows an oscillatory behaviour resulting from the pressure fluctuation above the sun-roof. This oscillatory behaviour gradually becomes weaken as one moves deeper into the car compartment. The acoustic pressure distribution along all vertical lines seems to show the corresponding behaviour in such a way that oscillatory effects deep inside the car compartment disappear. This shows that the solution obtained is reliable. The acoustic pressure tends to be more stable at the bottom of the car compartment. The computational results obtained from the test cases above have been presented in Lai, Lai, Pericleous, Djambazov [Lai et al, 2009].

4.3 Closure

A coupling method, in which the near-field of the unsteady flow is simulated by a fine-mesh-small-timestep-LES-alike numerical method applied in two-dimension, and the acoustic propagation is resolved by Helmholtz equation to predict buffeting noise inside a car compartment due to aerodynamic flow over an open sunroof, has been tested. The acoustic result obtained is believed to be reliable and appropriate.

In summary, a typical second order finite difference method for convection diffusion equations leads to a penta-diagonal linear system. Different high order schemes used in an unsteady Navier-Stokes problem generates different sparse structures for the linear systems. Handling different types of linear system may require different methods in order to achieve optimal speed. One disadvantage of developing high order schemes within a CFD software package is that it complicates the nonlinear and linear solver routines. However, new routines might be required, therefore, software re-use becomes extremely difficult. Data structure becomes a problem every time a new high order scheme is being introduced and deployed in the CFD software environment. Automation of software becomes difficult. In the next chapter, the framework of the DCM is to be used to improve software re-usability.

Chapter 5 THE DEFECT CORRECTION FRAMEWORK FOR PROBLEMS AT THE DISCRETISED LEVEL

As presented in the test case in last chapter, the buffeting noise along the sunroof is computed by solving an Implicit-LES-like method with high-order-scheme-filter-effect, instead of the classic LES supplemented with a sub-grid scale turbulent model, but in two-dimension. Fine time steps and spatial mesh are used. Spatial discretisation in higher order provides better numerical approximation than using 2nd order CFD schemes. This is in essence a LES, however, not strictly in its sense, since LES applies to Three Dimensional problem, but this is 2D.

High order schemes are usually very difficult to implement without significant re-arrangement of the linear equations. They require to have its matrix coefficients re-calculated and stored in data structures that may be very different from the existing schemes. Therefore it is necessary to write completely new codes and incorporate these codes into an existing CFD software in order to benefit the software platform. On the other hand high order schemes generate truncation terms which are not completely useful in the context of LES. This chapter examines the concept of an efficient implementation of high order schemes without interrupting the software platform and the related truncation errors in the context of LES. In later investigation attention is paid to the reasoning behind the use of filters, such as box and Gaussian filters, in LES and their relations with the truncation errors. It is an early attempt in this thesis to explore such relationship in order to provide a robust implicit-LES-like method for 2-D simulation.

This will provide an economical tool with quick turn-over of numerical experiments in identifying major possible noise sources.

5.1 Analysis of a One-Dimensional Problem

A steady state convection and diffusion problem of one dimension is given as

$$-\phi''(x)+a(x)\phi'(x)+b(x)\phi(x)= f(x,k,\alpha_k),\ x\in[0,1], \tag{5.1.1}$$

where $\phi(x)$ is the physical variable, $a(x)$ and $b(x)$ are two given functions of x and α_k is a sequence of random numbers in (0,1). The r.h.s. is defined as

$$f(x,k,\alpha_k) = \frac{8A\pi^3}{L^3}\sum_{k=0}^{N} k^3 \sin\left(\frac{2\pi kx}{L}+\pi\alpha_k\right) + \frac{4A\pi^2}{L^2}a(x)\sum_{k=0}^{N} k^2\cos\left(\frac{2\pi kx}{L}+\pi\alpha_k\right)$$

$$+\frac{2A\pi}{L}b(x)\sum_{k=0}^{N} k\sin\left(\frac{2\pi kx}{L}+\pi\alpha_k\right). \tag{5.1.2}$$

Here A is the amplitude, L is the size of the domain, and N is a value normally chosen as half of the number of grid points. In the test below the values of A and L are chosen as 1. The boundary conditions for the problem in Equation (5.1.1) are chosen as $\phi(0)=\sum_{k=0}^{N} 2\pi k\sin\pi\alpha_k$ and $\phi(1)=\sum_{k=0}^{N} 2\pi k\sin(2\pi k+\pi\alpha_k)$.

This problem has analytical solution (see Figure 5.1)

$$\phi(x)=\sum_{k=0}^{k=N} A\,2\pi k/L\,\sin\left(2\pi kx/L+\pi\alpha_k\right) \tag{5.1.3}$$

Note that the analytical solution, which involves a function of *sin*, is to mimic the artificial sinusoidal vertical-velocity disturbance that is used to represent a single vortex at the upstream of the car configuration in the previous car sunroof problem.

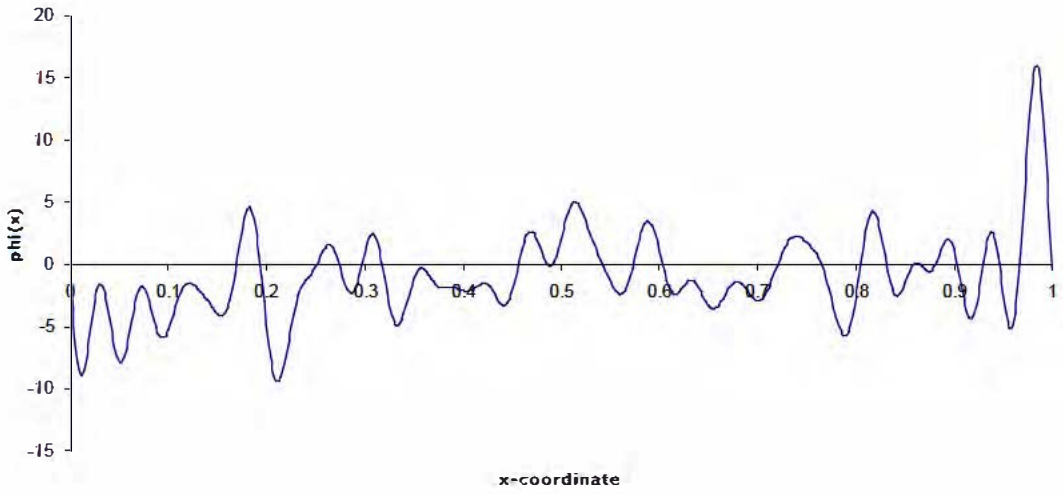

Figure 5.1: Analytical solution for the one dimensional problem with N = 201

Obtaining different high order finite difference discretisations for equation (5.1.1) is a tedious task affecting the software development. A systematic algorithm has been developed for an easy implementation of high order schemes based on the concept of the defect correction method.

Taylor's Series Expansion of ϕ_{i+1} and ϕ_{i-1} lead to

$$\phi_{i+1} = \phi_i + h\phi_i' + \frac{h^2}{2!}\phi_i'' + \frac{h^3}{3!}\phi_i''' + \frac{h^4}{4!}\phi_i^{(4)} + \frac{h^5}{5!}\phi_i^{(5)} + \frac{h^6}{6!}\phi_i^{(6)}, \tag{5.1.4}$$

$$\phi_{i-1} = \phi_i - h\phi_i' + \frac{h^2}{2!}\phi_i'' - \frac{h^3}{3!}\phi_i''' + \frac{h^4}{4!}\phi_i^{(4)} - \frac{h^5}{5!}\phi_i^{(5)} + \frac{h^6}{6!}\phi_i^{(6)}. \tag{5.1.5}$$

where h is the step size and ϕ_i', ϕ_i'', ..., $\phi_i^{(6)}$ represent the first, second and up to sixth orders of accuracy.

Adding Equation (5.1.4) and (5.1.5) to obtain the second derivative as in Equation (5.1.6), and subtracting Equation (5.1.5) from (5.1.4) to obtain the first derivative as in Equation (5.1.7).

$$\phi_i'' = \frac{\phi_{i-1} - 2\phi_i + \phi_{i+1}}{h^2} - \frac{h^2}{12}\phi_i^{(4)} - \frac{h^4}{360}\phi_i^{(6)} + O\left(h^6\right), \tag{5.1.6}$$

$$\phi_i' = \frac{\phi_{i+1} - \phi_{i-1}}{h} - \frac{h^2}{6}\phi_i''' - \frac{h^4}{120}\phi_i^{(5)} + O\left(h^6\right) \tag{5.1.7}$$

Substitute Equation (5.1.6) and (5.1.7) into Equation (5.1.1), one gets

$$\left(-\frac{1}{h^2}-\frac{a(x)}{2h}\right)\phi_{i-1}+\left(\frac{2}{h^2}+b(x)\right)\phi+\left(-\frac{1}{h^2}+\frac{a(x)}{2h}\right)\phi_{i+1}+\tau_i=f_i, \tag{5.1.8}$$

where τ_i is the high order truncation term form the Taylor's series expansion. Hence for 2nd order accuracy of the approximation used in (5.1.8) one has the truncation denoted as $\tau_i^{(2)}=0$; for 4th order $\tau_i^{(4)}=\frac{h^2}{12}\phi_i^{(4)}-a(x)\frac{h^2}{6}\phi_i'''$ and for 6th order $\tau_i^{(6)}=\frac{h^2}{12}\phi_i^{(4)}+\frac{h^4}{360}\phi_i^{(6)}+a(x)\left(-\frac{h^2}{6}\phi_i'''-\frac{h^4}{120}\phi_i^{(5)}\right)$.

According to the DCM, to ease the complexity and obtain the flexibility of the software implementation, one can solve for an approximated solution and then calculate for a correction using the same form to obtain the final solution. Rearrange Equation (5.1.8) as making ϕ_i to be the resolved variable, one gets

$$L\phi_i^*=L_h\phi_i^*+\tau_i=f_i, \tag{5.1.9}$$

where ϕ_i^* is the resolved solution. To achieve an approximate solution $\overline{\phi_i}$, the program can be used to solve

$$L_h\overline{\phi_i}=f_i. \tag{5.1.10}$$

Subtract Equation (5.1.10) from (5.1.9) one gets,

$$L_h\widetilde{\phi_i}=-\tau_i \tag{5.1.11}$$

where

$$\widetilde{\phi_i}=\phi_i^*-\overline{\phi_i} \tag{5.1.12}$$

Hence, one can use the same program as used to calculate $\overline{\phi_i}$ to calculate the "correction" $\widetilde{\phi_i}$ in order to obtain the final solution $\phi_i^*=\overline{\phi_i}+\widetilde{\phi_i}$.

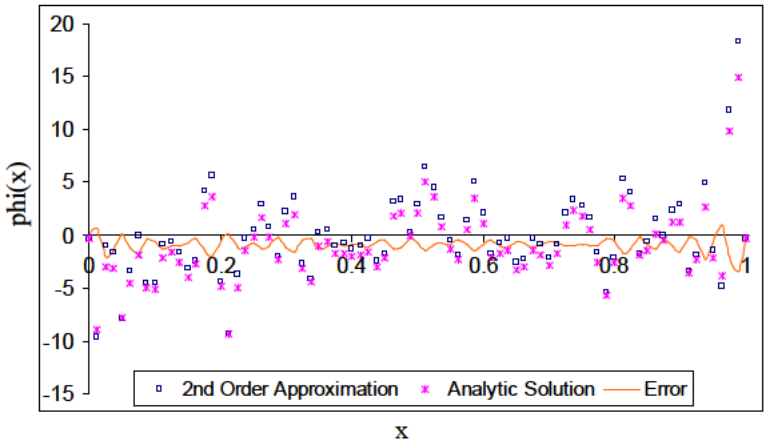

Figure 5.2: Numerical approximation solution with step-size $\delta x = 1.25e^{-2}$ against analytical solution. Numerical solution to 2nd order accuracy

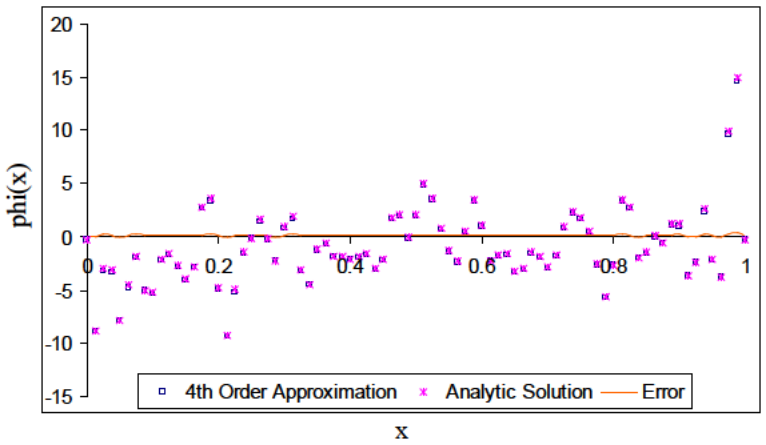

Figure 5.3: Numerical solution to 4th order accuracy

The results from the comparison are shown in Figure 5.2 and Figure 5.3. As expected, higher order (4th order in this case) approximation improves the accuracy of the numerical calculation.

5.2 Filtering Effects

In the early attempt in this thesis it provides a robust implicit-LES-like method for 2-D simulation on car sun-roof buffeting problem. The LES equations are derived from filtering the Navier-Stokes equations. The numerical solution of these equations is usually intractable in turbulent flow, due to the large range of scales of motion. To reduce this range, the equations are filtered. The purpose of introducing the filtering effect is to filter out the smaller scales of motion from the solution field. Thus, in LES the large

scale motions of the flow are calculated, while the effect of the smaller universal scales (the sub-grid scales) are modelled using a sub-grid scale (SGS) model.

The DCM resembles how filtering is coded in Large Eddy Simulations. Treating $\overline{\phi}_i$ as the large scale component similar to those that would be resolved by solving unsteady Navier-Stokes equations with a small temporal step, $\widetilde{\phi}_i$ then becomes the small scale (filtered-out) component which would be modelled by a sub-grid scale model.

High order schemes with fine temporal and spatial mesh should resemble the filtering in LES. The DCM described above may be considered as extracting information from a sub-grid model. In this study, the high order schemes were compared with the similar filtering effect employed in LES and their similarities were demonstrated by using a couple of common filters.

In order to compare which type of filter has the similar filter effect with which high order scheme, two types of common used filters, Box filter and Gaussian filter, has applied on analytical solution to compare the effects.

Box filtering, also known as mean filtering, is a simple, intuitive and easy to implement method of reducing the amount of intensity variation between one pixel of a picture and the next to smooth the image.

The idea of box filtering is simply to replace each pixel value in an image with the mean ("average") value of its neighbours, including itself. This has the effect of eliminating pixel values which are unrepresentative of their surroundings. Box filtering is usually thought of as a convolution filter, which is based around a kernel that represents the shape and size of the neighbourhood to be sampled when calculating the mean.

The Gaussian filtering is a different type of convolution filter, which is used in image processing to "blur" images and remove detail and noise, and in fluid dynamic to damp-out fluctuations (small scales) in CFD simulation. In this sense it is similar to the box filter, but it uses a different kernel that represents the shape of a Gaussian ("bell-shaped") hump.

The Gaussian distribution in one dimensional has the form:

$$G(x) = \frac{1}{\sqrt{2\pi}\sigma} e^{-\frac{x^2}{2\sigma^2}}, \tag{5.1.13}$$

where σ is the standard deviation of the distribution and x is the spatial coordinate. Here one can assume the distribution has a mean of zero (i.e. it is centred on the line x=0).

After applying each filter onto the analytical solution, results are shown in Figure 5.4 and Figure 5.5.

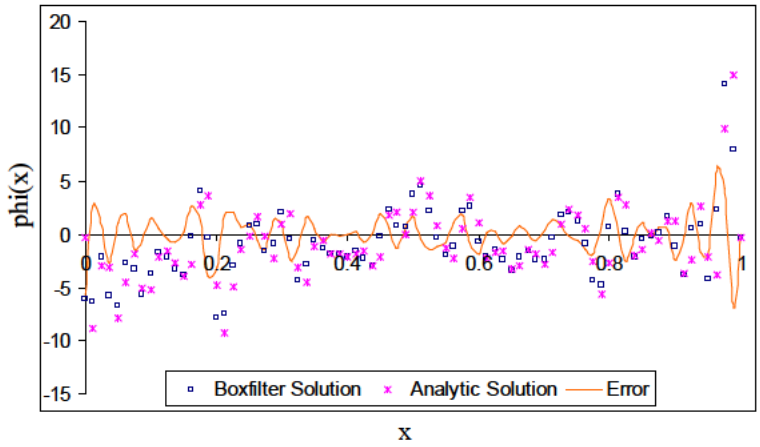

Figure 5.4: Filtered solution with filter-size $\Delta x = 1.25e^{-2}$ against analytical solution – Box filter

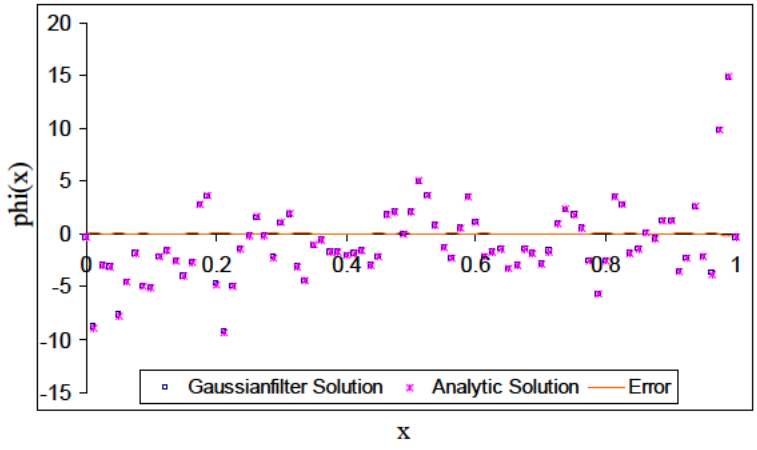

Figure 5.5: Filtered solution with filter-size $\Delta x = 1.25e^{-2}$ against analytical solution – Gaussian filter

Comparing the two results, one finds that the result obtained by Gaussian filter has much less error than the one obtained by Box filter. The Gaussian filter outputs a "weighted average" of each grid point's neighbourhood, with the average weighted more towards the value of the central grid points. This is in contrast to the Box filter which uses

uniformly weighted average. Hence Gaussian filter provides gentler smoothing and preserves fluctuations and peaks up to certain frequency better than a similarly sized Box filter.

Based on these investigations, there seems to be a certain relationship between a given high order scheme with a mesh size and the effect of a filter. As shown in previous comparison, it is not difficult to notice that both 4^{th} order accuracy numerical approximation and Gaussian filtered solution show good agreement with the analytical solution roughly on the same level. Same observation applies to 2^{nd} order accuracy numerical approximation and Box filtered solution, however, they show agreement with the analytical solution respect to a larger scale. From the comparison of their total errors from analytical solution (see Table 5.1), it is very interesting to see that similarities between 2^{nd} order numerical solution and Box filtered solution, as well as between 4^{th} order numerical solution and Gaussian filtered solution, are observed while both step-sizes applied are twice as big as both filter-sizes (i.e. $\delta x = 2\Delta x$). Further investigation and more test cases are needed to explore the relationship between higher order numerical schemes and filtering effects.

Boxfilter				2nd Order		
	Filter Size Δx	||U_flt(i) - Ua(i)||_2		Step Size dx	||U_h(i) - Ua(i)||_2	
n=11	0.1	2.551884764		0.1	422.7291068	
n=21	0.05	2.883142985		0.05	530.727447	
n=41	0.025	2.164919375		0.025	8.30003448	
n=81	0.0125	1.907324303		0.0125	1.103341259	When dx = 2Δx
n=161	0.00625	1.008744755		0.00625	0.241058931	
n=201	0.005	0.81289721		0.005	0.151947601	
Gaussianfilter				4th Order		
	Filter Size Δx	||U_flt(i) - Ua(i)||_2		Step Size dx	||U_h(i) - Ua(i)||_2	
n=11	0.1	0.868686429		0.1	5470.289317	
n=21	0.05	0.388194824		0.05	1196.676821	
n=41	0.025	0.122649006		0.025	4.942043652	
n=81	0.0125	0.048486014		0.0125	0.135722336	When dx = 2Δx
n=161	0.00625	0.193633671		0.00625	0.007138155	When dx = 2Δx
n=201	0.005	0.006810992		0.005	0.002866702	

Table 5.1: Comparison of total errors between high order (2^{nd} and 4^{th} order) numerical approximations and analytical solution, as well as filtered (Box filter and Gaussian Filter) solutions and analytical solution

5.3 Closure

A simple one dimensional numerical example has been resolved by using DCM up to 4^{th} and 6^{th} order of accuracy. 2^{nd} and 4^{th} order schemes are compared with two different types of filtering effects: Box and Gaussian filters; and similarity between them has been discussed. The use of DCM has been tested initially to become a possible concept of re-use existing CFD linear solvers without affecting the data structure of the software.

Chapter 6 CONCLUSION AND FUTURE WORK

This thesis examines a general framework of the DCM. The principle of the method is described and the concept is demonstrated using various examples. The framework is then extended to simple perturbation problems that exhibit multiple scales at the continuum level. One key advantage of the framework is to allow multi-scale problems to be implemented easily using existing commercial fluid dynamics and CFD packages.

The framework can be applied to direct sound computation techniques such as Reynolds averaged Navier-Stokes equations and Large Eddy Simulation, and also to the Lighthill's Acoustic Analogy. It shows the applicability of the framework that is suitable for all the development has been built. In particular, the derivation of Lighthill's Acoustic Analogy has demonstrated a much simpler approach to resolve the flow's compressible counterparts without solving the more complicated wave equation in a separate solver.

A coupling method, in which the near-field of the unsteady flow is simulated by a fine-mesh-small-timestep-LES-alike numerical method applied in two-dimension, and the acoustic propagation in the far-field is resolved by Helmholtz equation to predict buffeting noise inside a car compartment due to aerodynamic flow over an open sunroof, has been tested in this thesis. The acoustic result obtained is believed to be reliable and appropriate. A comparison between the filtering effect and the use of high order schemes has successfully illustrated the relation between them. This has further demonstrated that such LES-alike method which uses high order scheme in its calculation is an appropriate and effective way of achieving similar result as the original LES method with relatively less computational time [Sagaut, 2006]. From this exercise, it is observed that different high order schemes used in an unsteady Navier-Stokes problem generates different sparse

structures for the linear systems. Different sparseness of the linear system requires different linear solvers in order to achieve optimal speed of convergence. The automation of software and software re-usability is most effected each time when a new compact high order scheme is developed. The approach described in this thesis opens an opportunity for a flexible choice of the order of accuracy without increasing the additional work in implementing algorithm within the existing software environment. In other words automation of software is enhanced.

The use of DCM opens a new way of software re-use without major amendments to data structure within each software coding. Evaluation of the defect can be done without affecting the data structure of the linear solver.

For future work, thorough comparison between high order schemes and filtering process needs to be conducted. Further tests on higher order scheme (6^{th} and 8^{th} order) and compare results with other type of filters. Such tests can also be extended to 2-D or 3-D problems. Several 2-D buffeting noise test examples and time dependent test problems are to be examined using a variety of different high order schemes, and their filtering effects are to be summarised whilst looking for a possible alternative for sub-grid modelling. An implementation based on the framework of DCM should be built into an existing industrial CFD software so that it no longer needs to rely on an external coupling technique to resolve the acoustic perturbations in the near field. On the other hand high order schemes based on the defect correction principle should also be incorporated into existing software with the possibility of sub-grid modelling based on the investigation in Chapter 5 allowing an easy approach to LES-like methods. By implementing this within the CFD commercial software, it would bring computational benefits. Exploring into other industrial related problems, involving multiscale and high order schemes, where the use of the DCM framework can be expanded.

REFERENCES

[1] Auzinger, W., Koch, O. and Weinmuller, E., "New Variants of Defect Correction for Boundary Value Problems in Ordinary Differential Equations", Vienna University of Technology, ANUM Preprint, 2002

[2] Baysal, O., Yen, G.W. and Fouladi, K., "Navier-Stokes Computations of Cavity Aeroacoustics with Suppression Devices", AIAA/DGLR Paper 92-02-161, 1992

[3] Böhmer, K., "Defect Corrections via Neighbouring Problems". I. General Theory. MRC Report, University of Wisconsin-Madison No. 1750, 1977

[4] Böhmer, K., "Discrete Newton Methods and Iterated Defect Corrections", I. General Theory, h. Initial and Boundary Value Problems in Ordinary Differential Equations. Berichter Nr.10,11, Universitat Karlesruhe, Fakultät für Manthematik, 1978

[5] Böhmer, K., "Discrete Newton Methods and Iterated Defect Corrections", Numer. Math.37, 167-192, 1981

[6] Böhmer, K., and Stetter, H.J., editors. "Defect Correction Methods: Theory and Applications", Springer-Verlag, Wien, 1984

[7] Breuer, M., "A Challenging Test Case for Large Eddy Simulation: High Reynolds Number Circular Cylinder Flow", International Journal of Heat and Fluid Flow 21, 648-654, 2000

[8] Ciardi, M., Sagaut, P., Klein, M. and Dawes, W.N., "A Dynamic Finite Volume Scheme for Large-Eddy Simulation on Unstructured Grids", Journal of Computational Physics, 210, pp. 632-655, 2005

[9] Djambazov, G.S., Lai. C.–H., and Pericleous, K.A., "Development of A Domain Decomposition Method for Computational Aeroacoustics", in Bjørstad, P.E., Espedal, M.S. and Keyes, D.E., editors, Domain Decomposition Methods in Science and Engineering. John Wiley & Sons, 1997. Proceedings from the Ninth International Conference, Bergen, Norway , June 1996

[10] Djambazov, G.S., Lai, C.–H., and Pericleous, K.A., "Efficient Computation of Aerodynamic Noise", in Mandel, J., Farhat, C. and Cai, X.–C, editors, Tenth

International Conference on Domain Decomposition Methods, pp. 506-512. AMS, Contemporary Mathematics 218, 1998

[11] Dubsky, J., "Aeroacoustic Noise From A Car Sunroof", MEng Project, University of Exeter, 2003

[12] Dutt, A., Greengard, L., Rokhlin, V., "Spectral Deferred Correction Methods for Ordinary Differential Equations", BIT, 11, No. 2, pp. 241-266, 2000

[13] Ervin, V., Layton, W., Maubach, J., "Adaptive Defect Correction Methods for Viscous Incompressible Flow Problems", SIAM J. Numer. Anal., 37, pp. 1165-1185, 2000

[14] Ervin, V., Lee, H.K., "Defect Correction Method For Viscoelastic Fluid Flows at High Weissenberg Number", Numerical Methods for Partial Differential Equations, Volume 22, Issue 1, pp. 145-164, 2006

[15] Ewert, R. and Schroder, W., "Acoustic Perturbation Equation Based on Flow Decomposition via Source Filtering", Journal of Computational Physics, Vol 188, Issue 2, 365-398, 2003

[16] Ffowcs–William, J.E. and Hawkings, D.L., "Sound Generated by Turbulence and Surfaces in Arbitrary Motion", Philosophical Transactions of the Royal Society of London, Vol. 264A, pp. 321-342, 1969

[17] Ffowcs–William, J.E., "Hydrodynamic Noise", Annual Review of Fluid Mechanics, Vol. 1, Issue 1, pp. 197-222, 1969

[18] Fox, L., "Some improvements in the use of relaxation methods for the solution of ordinary and partial differential equations", Proceedings of the Royal Society of London, A 190 (1020), 31-59, 1947

[19] Frank, R., Ueberhuber, C.W., Iterated Defect Correction for the Efficient Solution of Stiff Systems of Ordinary Differential Equations", BIT 17, 146-159, 1977

[20] Green, G., "An Essay on the Application of Mathematical Analysis to the Theories of Electricity and Magnetism", Printed by T. Wheelhouse, Nottingham, 1828

[21] Gulick, W.L., "Hearing: Physiology and Psychophysics.", Oxford Univ. Press, London and New York, 1971

[22] Hardin, J.C. and Lamkin, S.L., "Aeroacoustic Computation of Cylinder Wake Flow", AIAA Journal, 22 (1, pp. 51-57), 1984

[23] Heinrichs, W., “Defect Correction for Convection Dominated Flow”, SIAM J. Sci. Comput., 17, 1082-1091, 1996

[24] Hemker, P.W., Shishkin, G.I., Shishkina, L.P., “The Use of Defect Correction for the Solution of A Singularly Perturbed O.D.E.”, ZAMM • Z, angew. Math. Mech. Vol. 77, No. 1, pp. 59-74, 1997

[25] Hemker, P.W., Shishkin, G.I., Shishkina, L.P., “High-Order Time-Accurate Schemes for Singularly Perturbed Parabolic Convection-Diffusion Problems with Robin Boundary Conditions”, Computational Methods in Applied Mathematics, Vol. 2, No. 1, pp. 3-25, 2002

[26] Heywood, J., Rannacher, R., “Finite-Element Approximations of the Non-stationary Navier-Stokes Problem. Part 4: Error Analysis for Second-Order Time Discretization”, SIAM J. Numer. Anal., 2, 1990

[27] Hsi, F.Q. and Perie, F., “Computational Aeroacoustics for Prediction of Acoustic Scattering”, Proceedings Second Computational Aeroacoustics workshop on Benchmark Problems, NASA CP 3352, pp. 111-117, 1977

[28] Inagaki, M., Murata, O., Kondoh, T. and Abe, K., “Numerical Prediction of Fluid-Resonant Oscillation at Low Mach Number”, AIAA Journal, Vol.40, pp. 1823-1829, 2002

[29] Kirchhoff, G.R., “Toward a Theory of Light Rays”, Annals of Physical Chemistry, Vol. 18, pp. 663-695, 1883

[30] Koren, B., “Multigrid and Defect-Correction for the Steady Navier-Stokes Equations”, Applications to Aerodynamics, S. W. I. Track 74, Centrum voor Wiskunde en Informatica, Amsterdam, 1991

[31] Labovschii, A., “A Defect Correction Method for the Time-Dependent Navier-Stokes Equations”, Numerical Methods for Partial Differential Equations, Volume 25, Issue 1, pp. 1-25, 2009

[32] Lai, L.S., Lai, C.–H., Pericleous, K.A., Djambazov, G.S., “Comparison of Higher-Order Numerical Schemes and Several Filtering Methods Applied to Navier-Stokes

Equations with Applications to Computational Aeroacoustics", Journal of Algorithms and Computational Technology, 3 (3), 443 – 459, 2009

[33] Lallemand, M.–H., Koren, B., "Iterative Defect Correction and Multi-grid Accelerated Explicit Time Stepping Schemes for the Steady Euler Equations", SIAM Journal on Scientific Computing, vol. 14, Issue 4, 1993

[34] Launder, B.E., Reece, G.J. and Rodi, W., "Progress in the Development of a Reynolds Stress Turbulence Closure", J. Fluid Mech., 68, 537-566, 1975

[35] Launder, B.E. and Spalding, D.B., "Mathematical Models of Turbulence", Academic Press, 1972

[36] Layton, W., Lee, H.K., Peterson, J., "A Defect Correction Method for the Incompressible Navier-Stokes Equation", Applied Mathematics and Computation, Vol. 129, Issue 1, pp. 1-19, 2002

[37] Lighthill, J.M., "On Sound Generated Aerodynamically. Part I Generally Theory", Proceedings of the Royal Society, Vol. 211A, pp. 564-587, 1952

[38] Lilley, G., "On the Noise from Jets", AGARD CP-131, PP. 13.1-13.10, 1974

[39] Liu, Q. and Hou, Y., "A Two-Level Defect-Correction Method for Navier-Stokes Equation", Bulletin of the Australian Mathematical Society, Vol. 81, Issue 03, 442-454, 2010

[40] Manoha, E., Elias, G., Troff, B., Sagaut, P., "Towards the Use of Boundary Element Method in Computational Aeroacoustics", AIAA Paper 99-1980, 1999

[41] Moeng, C.-H. and Sullivan, P.P., "Large Eddy Simulation", Encyclopedia of Atmospheric Sciences, pp. 1140-1150, 2002

[42] Minion, M.L., "Semi-Implicit Projection Methods for Incompressible Flow Based on Spectral Deferred Corrections", Appl. Numer. Math., 48(3-4), 369-387, 2004

[43] Nieuwstadt, F.T.M., Mason, P.J., Moeng, C.-H., and Schumann, U., "Large Eddy Simulation of the Convective Boundary Layer: A Comparison of Four Computer Codes", in Durst et al., Turbulent Shear Flows, Vol. 8, Springer-Verlag, Berlin, 431 pp., 1993

[44] Orszag, S.A. and Patterson, G.S., "Numerical Simulation of Turbulence: Statistical Models and Turbulence", Lecture Notes in Physics 12, 127-147, Springer-Verlag, Berlin, 1972

[45] Patankar, V., "Numerical Heat Transfer and Fluid Flow", Hemisphere, Washington, DC, 1980

[46] Pereyra, V., "On Improving the Approximate Solution of a Functional Equation by Deferred Corrections", Numer. Math, 8, pp. 376-391, 1966

[47] Pereyra, V., "Iterated Deferred Correction for Nonlinear Boundary Value Problems", Numer. Math, 11, pp. 111-125, 1969

[48] PHOENICS, www.cham.co.uk

[49] Pilon, A.R. and Lirintzis, A., "Development of an Improved Kirchhoff Method for Jet Aeroacoustics", AIAA Journal, Vol.36, pp.783-790, 1998

[50] PowerFLOW & PowerACOUSTICS, www.exa.com

[51] Qin, Y., Zeng, D. and Wu, K., "A Defect-Correction Method Based on Equal-Order Finite Elements for the Incompressible Flows", Multimedia Technology (ICMT) International Conference, pp 2351 – 2354, 2011

[52] Ricot, D., Maillard, V. and Bailly, C., "Numerical Simulation of the Unsteady Flow Past a Cavity and Application to the Sunroof Buffeting", American Institute of Aeronautics and Astronautics, 2001-2112, 2001

[53] Rossing, T.D., "The Science of Sound", Addison-Wesley, Reading, Massachusetts, 1982

[54] Sagaut, P., "Large Eddy Simulation for Incompressible Flows – Third Edition", Springer, ISBN 3-540-26344-6, 2006

[55] Shih, S.H., Hamed, A., and Yeuan, J.J., "Unsteady Supersonic Cavity Flow Simulation Using Coupled k-e and Navier-Stokes Equations", AIAA Journal, Vol. 32, No.10, pp. 815-913, 1994

[56] Stetter, H.J., "Economical Global Error Estimation", R. A. Willoughby (Ed.), Stiff Differential Systems, pp. 245-258, 1974

[57] Stetter, H.J., "The Defect Correction Principle and Discretization Methods", Numer. Math. 29, 425-443, 1978

[58] Stevens, S.S. and Davis, H., “Hearing: Its Psychology and Physiology.”, Wiley, New York, 1938, American Institute of Physics, New York, reprinted 1983

[59] Tam, C.K.W., “Computational Aeroacoustics: An Overview”, RTO AVT Symposium on “ Ageing Mechanisms and Control: Part A – Developments in Computational Aero- and Hydro-Acoustics”, 2001, RTO-MP-079

[60] Vasilyev, O.V., Lund, T.S., and Moin, P, “A General Class of Commutative Filters for LES in Complex Geometries”, Journal of Computational Physics, 146, 82-104, 1998

[61] Viswanathan, K. and Sankar, L.N., “Toward the Direct Calculation of Noise: Fluid/Acoustic Coupled Simulation”, AIAA Journal, Vol. 33, No.12, pp 2271-2279, 1995

[62] Wang, Z.K., “A Source-extraction Based Coupling Method for Computational Aeroacoustics”, Ph.D. Thesis, University of Greenwich, 2004

[63] Wang, Z.K., Djambazov, G., Lai, C.-H. and Pericleous. K., “Numerical Simulation of Flow-Induced Cavity Noise in Self-Sustained Oscillations”, Comput Visual Sci 10, pp 123-134, 2007

[64] Wilkinson, J.H., “Rounding Errors in Algebraic Processes”, Englewood Cliffs, NU: Prentice Hall, 1963

[65] Wood, A.B., “A Textbook of Sound”, Bell, London, 1946

[66] Zadunaisky, P., “A Method for the Estimation of Errors Propagated in the Numerical Solution of a System of Ordinary Differential Equations”, G. Contopoulus (Ed.), The Theory of Orbits in the Solar System and in Stellar Systems. Proceedings of International Astronomical Union, Symposium 25, 1964

[67] Zadunaisky, P., “On the Estimation of Errors Propagated in the Numerical Integration of Ordinary Differential Equations”, Numer. Math. 27, 21-39, 1976